JOURNAL OF GEOPHYSICAL RESEARCH, VOL. 103, NO. C10, PAGES 21,499–21,529, SEPTEMBER 15, 1998

Mixing of a tracer in the pycnocline

James R. Ledwell
Department of Applied Ocean Physics and Engineering, Woods Hole Oceanographic Institution
Woods Hole, Massachusetts

Andrew J. Watson
School of Environmental Sciences, University of East Anglia, Norwich, England, United Kingdom

Clifford S. Law
Plymouth Marine Laboratory, Plymouth, England, United Kingdom

Abstract. A patch of sulfur hexafluoride was released in May 1992 in the eastern North Atlantic on an isopycnal surface near 300 m depth and was surveyed over a period of 30 months as it dispersed across and along isopycnal surfaces. The diapycnal eddy diffusivity K estimated for the first 6 months was 0.12 ± 0.02 cm^2/s, while for the subsequent 24 months it was 0.17 ± 0.02 cm^2/s. The vertical tracer distribution remained very close to Gaussian for the full 30 months, as the root mean square (rms) dispersion grew from 5 to 50 m. Lateral dispersion was measured on several scales. The growth of the rms width of the tracer streaks from less than 100 m to approximately 300 m within 2 weeks implies an isopycnal diffusivity of 0.07 m^2/s at scales of 0.1 to 1 km, larger than expected from the interaction between vertical shear of the internal waves and diapycnal mixing. Teasing of the overall patch, initially about 25 km across, into streaks with an overall length of 1800 km within 6 months supports predictions of exponential growth by the mesoscale strain field at a rate of $3 \pm 0.5 \times 10^{-7}$ s^{-1}. The rms width of these streaks, estimated as 3 km and maintained in the face of the streak growth, indicates an isopycnal diffusivity of 2 m^2/s at scales of 1 to 10 km, much greater than expected from internal wave shear dispersion. The patch was painted in, albeit streakily, by 12 months, confirming expectations from analytical and numerical models. Homogenization of the patch continued during the subsequent 18 months, while the patch continued to spread with an effective isopycnal eddy diffusivity on the order of 1000 m^2/s, acting at scales of 30 to 300 km.

1. Introduction

The circulation of the ocean is severely constrained by density stratification. A water parcel cannot move from one surface of constant potential density to another without changing its salinity or its potential temperature. There are virtually no sources of heat outside the sunlit zone and away from the bottom where heat diffuses from the lithosphere, except for the interesting hydrothermal vents in special regions. The sources of salinity changes are similarly confined to the boundaries of the ocean. If water in the interior is to change potential density at all, it must be by mixing across density surfaces (diapycnal mixing) or by stirring and mixing of water of different potential temperature and salinity along isopycnal surfaces (isopycnal mixing).

Paper number 98JC01738.
0148-0227/98/98JC-01738$09.00

Most inferences of dispersion parameters have been made from observations of the large-scale fields or from measurements of dissipation rates at very small scales. Unambiguously direct measurements of the mixing have been rare. Because of the stratification of the ocean, isopycnal mixing involves very different processes than diapycnal mixing, extending to much greater length scales. A direct approach to the study of both isopycnal and diapycnal mixing is to release a tracer and measure its subsequent dispersal. Such an experiment, lasting 30 months and involving more than 10^5 km^2 of ocean, is the subject of this paper.

Tracer release experiments in the stratified ocean on 1-km scales performed with fluorescent dyes have revealed much about the phenomena of diapycnal mixing and the early stages of isopycnal mixing [*Woods*, 1968; *Schuert*, 1970; *Ewart and Bendiner*, 1981; *Vasholtz and Crawford*, 1985]. The introduction of sulfur hexafluoride (SF_6), detectable at concentrations a million times lower than the dyes, has made much larger experiments

possible [*Watson et al.*, 1987, 1991; *Wanninkhof et al.*, 1991]. Pilot experiments in deep, enclosed basins have proven the usefulness of SF_6 for measuring isopycnal and diapycnal mixing on timescales of weeks to years *Ledwell et al.*, 1986; *Ledwell and Watson*, 1991; *Ledwell and Hickey*, 1995; *Ledwell and Bratkovich*, 1995].

Water samples must be collected for shipboard analysis of SF_6 with present technology, so the spatial resolution of the technique is coarser than for dye, for which submersible fluorometers can sample several times a second. The strength of the SF_6 technique lies in the study of the longer-term, integrated, effects of the smaller-scale processes which are of relevance to the circulation of the ocean.

2. The Tracer

Sulfur hexafluoride is used extensively in industry and science as a gaseous dielectric [*Ko et al.*, 1993]. The extremely electrophilic nature of the compound makes it detectable in quantities as small as 10^{-17} mol with an electron-capture detector [*Lovelock and Ferber*, 1982]. Otherwise, SF_6 is extremely nonreactive at normal temperatures. It is safe to handle, except for its potential as an asphyxiant. It can be breathed by small mammals in a mixture of 80% SF_6 to 20% O_2 with no ill effects [*Lester and Greenberg*, 1950]. There is no reason to suspect it to be dangerous to marine organisms of any size, even at the concentrations reached in the injection plume of the experiments.

The production rate of SF_6 in 1990 was 5 to 8 x 10^6 kg/yr and has been estimated to be increasing at a rate of about 8% per year [*Maiss and Levin*, 1994]. Since it is an extremely volatile substance at normal conditions, all of the SF_6 produced escapes to the atmosphere within a few decades. The atmospheric inventory in 1990 was 6.3 x 10^7 kg. The solubility of SF_6 in seawater is low [*Wanninkhof et al.*, 1991], so that the concentration in the surface water of the ocean is presently of the order of 1 fM (1 fM = 1 femtomolar = 10^{-15} mol/L). The concentration decreases with depth [*Watson and Liddicoat*, 1985], the total burden in the ocean being of the order of 3 x 10^4 kg. The amount of SF_6 used for the present experiment was 139 kg, about 0.5% of this oceanic burden.

SF_6 does absorb infrared radiation, acting as a minor "greenhouse" gas in the atmosphere. However, at projected rates of emission its effect on warming over the coming decades will be negligible compared with the effect of the anticipated increase in atmospheric CO_2 [*Ko et al.*, 1993]. Its fate due to photolysis and other reactions in the upper atmosphere indicate a lifetime of many centuries [*Ko et al.*, 1993]. In summary, the impact on the marine and global environment of the use of SF_6 as an oceanic tracer is trivial. The main reason for moderation in its use is to avoid interference with future tracer experiments.

3. The Experiment

3.1. The Site

The North Atlantic Tracer Release Experiment (NATRE) took place in the southeastern part of the subtropical gyre, from early 1992 to late 1994 (Figure 1). Tracer was released at approximately 25°40' N, 28°15' W on a surface defined by a potential density of 1028.05 kg/m^3, referenced to 300 dbar. The corresponding potential density, referenced to atmospheric pressure, is approximately 1026.75 kg/m^3, i.e., $\sigma_\theta = 26.75$. The mean pressure on this surface at the release site during the release was 313 dbar.

This site was chosen as one of relatively low mesoscale eddy energy and small variations of temperature, salinity, and depth along isopycnal surfaces on scales of 100 km. The bottom depth near the site is generally greater than 5000 m. However, Great Meteor Seamount lies 450 km to the north, and an unnamed seamount with a peak at approximately 2000 dbar lies 200 km to the east. The prevailing flow in the region is to the southwest at speeds of around 1 cm/s [*Armi and Stommel*, 1983; *Thiele et al.*, 1986; *Bauer and Siedler*, 1988]. The site had the advantage of being in the center of an array of instruments deployed for an experiment to study the subduction of surface water into the pycnocline which was simultaneously performed [*Moyer and Weller*, 1997]. A set of five surface moorings were deployed for the subduction experiment to measure meteorological parameters as well as subsurface currents and temperatures. The instruments on the mooring at 25°32'N, 28°57'W (Figure 1), near the release site, were augmented with vector measuring current meters at depths of 300 and 310 m to study velocity and shear statistics at the level of the tracer release. Additional moorings were deployed in the region to track neutrally buoyant floats.

Profiles taken in the spring show the winter mixed layer underlying the developing seasonal pycnocline (Figure 2). The permanent pycnocline is located below about 200 dbar where the gradients undergo little seasonal change. Near 313 dbar, where the tracer was released, gradients change only slowly with depth. The buoyancy frequency N varies from 2.3 cph to 2.6 cph between 400 and 220 dbar, before increasing more sharply higher in the water column (Figure 3). The tracer was confined below this transition during the experiment. Of more significance is the variation in the density ratio R_ρ, the ratio of the stabilizing temperature gradient to the destabilizing salinity gradient:

$$R_\rho \equiv \frac{\alpha\,(\partial T/\partial z + \Gamma)}{\beta \partial S/\partial z} \qquad (1)$$

where T is the temperature, Γ is the adiabatic temperature gradient, z is the vertical coordinate, S is the salinity, $\alpha = -\rho^{-1}\partial\rho/\partial T$, $\beta = \rho^{-1}\partial\rho/\partial S$, and ρ is the

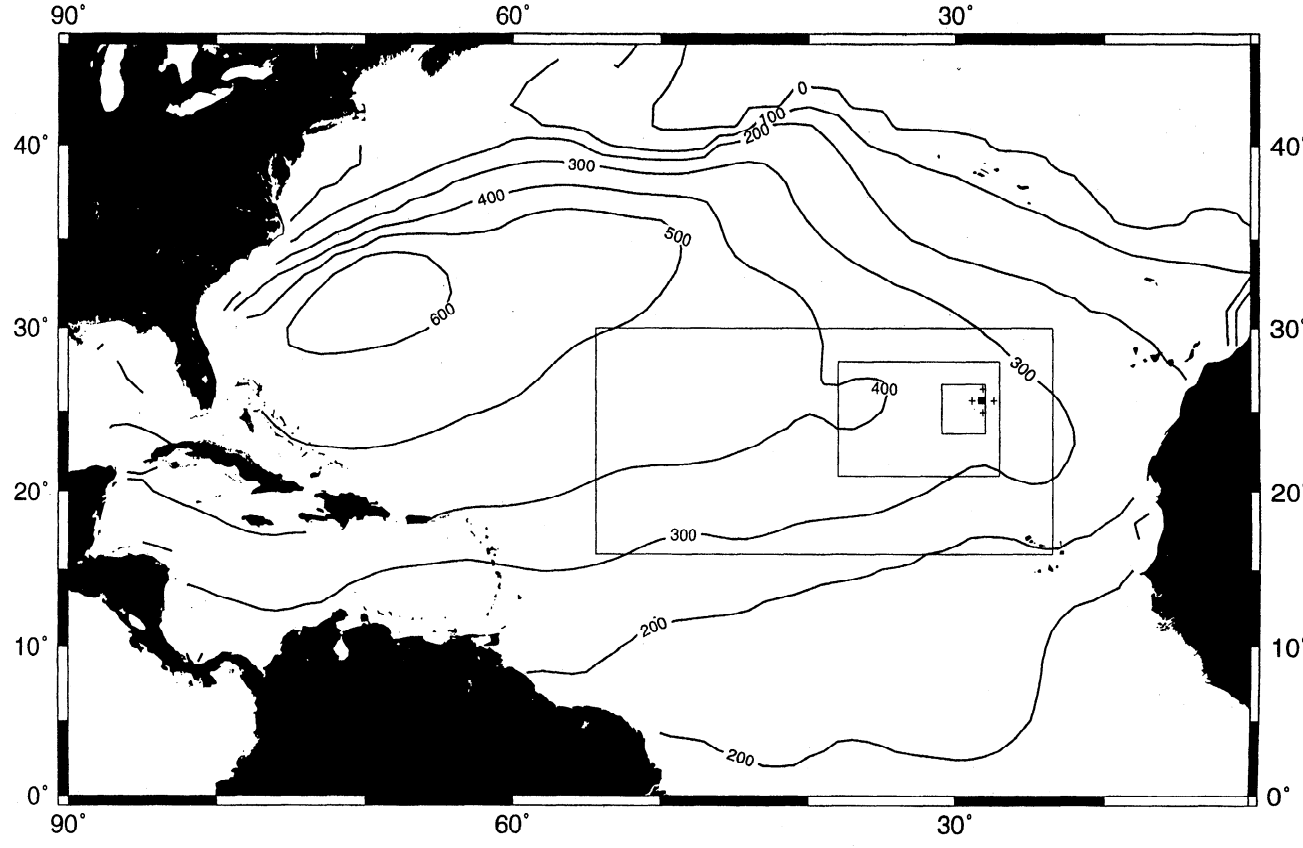

Figure 1. The site. The climatological mean depth of the target density surface for February-April from *Levitus* [1982] is contoured in meters. Square: tracer release area, May 1992 survey area, and central mooring for the Subduction Experiment; plus: background stations; rectangles: borders of maps showing data for fall 1992 (Figure 11), spring 1993 (Figure 19), and November 1994 (Figure 34) in order of increasing size.

density. Salt fingering is believed to play a role in diapycnal mixing in the ocean for R_ρ up to at least 2; well-defined salt fingering steps are often found for R_ρ less than about 1.6 [*Schmitt*, 1994]. In the present case, R_ρ decreases from a little less than 1.9 at 400 dbar to a little over 1.7 at 220 dbar.

3.2. Tracer Injection

A total of 139 ± 5 kg of SF_6 was released in a set of nine streaks between May 5 and 13, 1992, from R/V *Oceanus* (Figures 4a and 4b). The injection was performed by pumping liquid SF_6 through a pair of 50-μ diameter sapphire orifices at flow rates of 17 to 20 g/min and overpressures on the order of 10 MPa, while towing the injection system along the target density surface at a speed of approximately 0.5 m/s. The system included two nearly independent channels. When one channel failed, the most efficient action was often to continue with the other channel, rather than to recover the system immediately for repair. Thus, at some places along the streaks, the rate of tracer release was only half the maximum rate of 35 to 40 g/min.

The injection system was mounted on a 1 m x 1 m x 2.5 m long neutrally buoyant sled attached to the weighted hydrowire by a 2-m bridle. This bridle attenuated vertical motions of the wire at surface wave frequencies to a root mean square (rms) excursion of 0.07 m at the sled. Lower-frequency motions of the ship and of the target density surface relative to the sled were partially compensated by the winch, operating automatically in response to the error in potential density calculated at 6 Hz from conductivity, temperature, and pressure measured by a Sea-Bird 911plus CTD mounted on the sled. When the system strayed beyond a potential density window of ±0.01 kg/m^3, which occurred rarely, the injection pumps automatically turned off. The rms potential density error calculated from the CTD data for the entire injection was 0.0025 kg/m^3, equivalent to a depth error of 1.4 m in the mean vertical potential density gradient of 0.0018 kg/m^4. The turbulent wake of the injection sled, interacting with the hydrographic fine structure, is expected to have broadened the initial distribution of the tracer beyond this control error. However, extrapolation from the first sur-

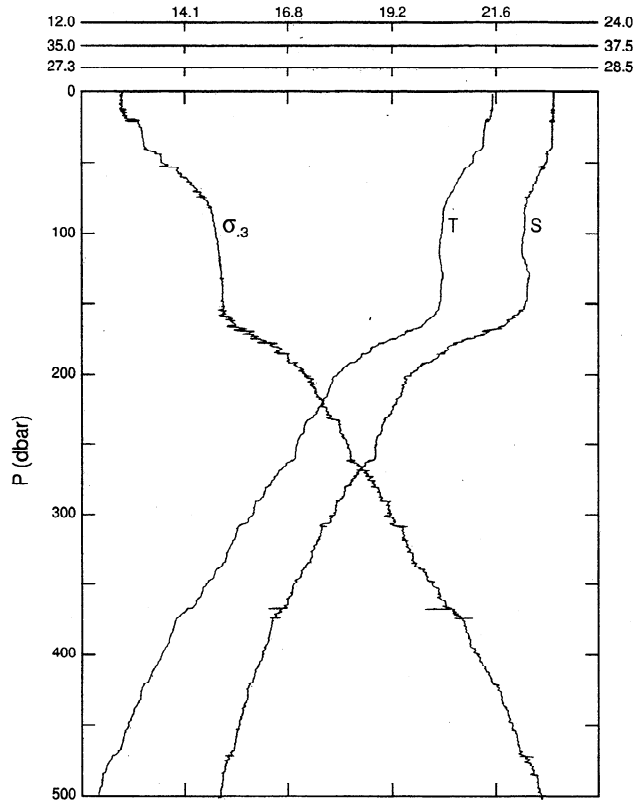

Figure 2. Typical CTD profile from the initial tracer survey, May 1992, unsmoothed. The axes at the top are for temperature (°C), salinity, and potential density anomaly referenced to 300 dbar.

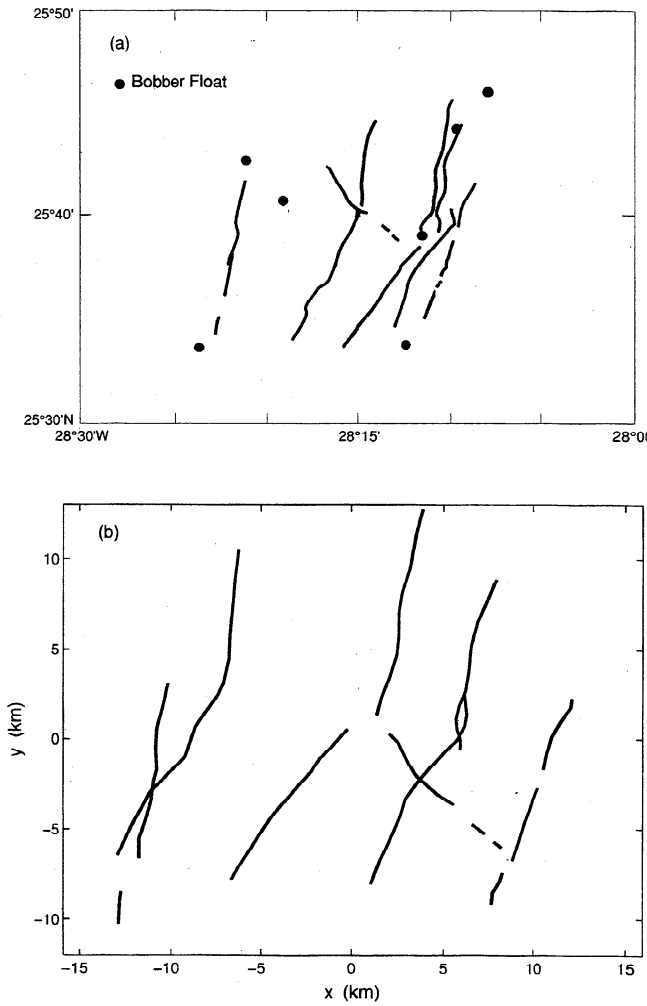

Figure 4. Initial tracer streaks and float positions: (a) in Earth-fixed coordinates; (b) relative to a neutrally buoyant float drifting with the patch. The Bobber Floats shown in Figure 4a were special layer-following floats released with the tracer for tracking and for the dispersion studies of *Sundermeyer and Price* [this issue].

vey back to the time of the injection suggests that the initial rms spread of the tracer was no greater than 2 m. Hence the injection appeared to be extremely well controlled, and the initial distribution of the tracer plume was tightly confined in density.

Neutrally buoyant floats were released with the tracer (Figure 4a) to aid in tracking the patch and to study lateral dispersion. They were accurately tracked at short range with high-frequency acoustics during injection and initial sampling and at long range with a SOFAR system for the first year of the experiment. Results from these floats are reported by *Sundermeyer and Price* [this issue].

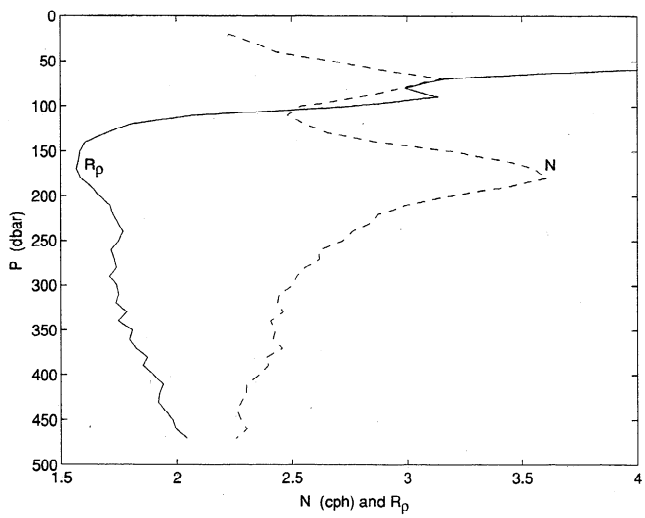

Figure 3. Mean buoyancy frequency and density ratio profiles from the May 1993 survey.

3.3. Background Samples

Profiles of the background concentration of SF_6 were obtained from four stations, 75 km north, south, east, and west of the release site, on May 13-14, 1992 from RRS *Charles Darwin* (Figures 1 and 5), and also from three stations north of the area of the tracer patch in spring 1993. The samples were analyzed by gas chromatography with an electron capture detector [*Law et al.*, 1994]. These low concentration samples were run by the sparge and trap technique applied to 350-ml aliquots from glass bottles that had been filled from 5-l Niskin bottles [Law et al., 1994]. The minimum detectable

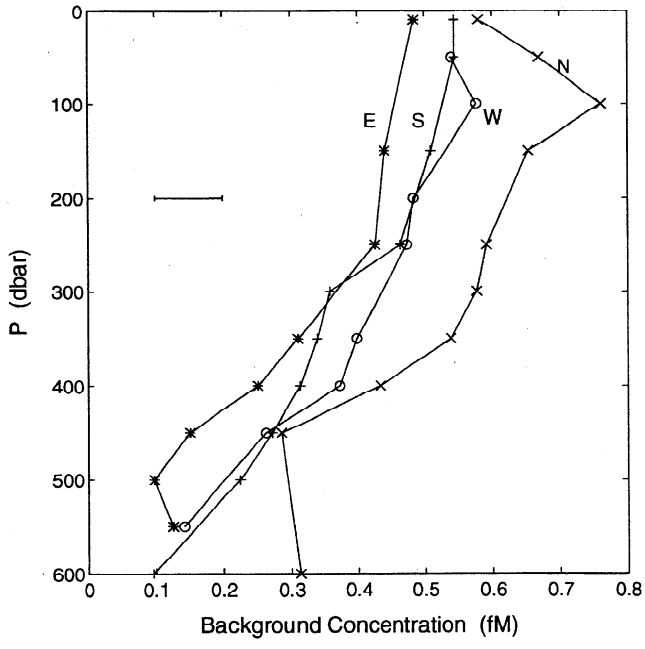

Figure 5. Background profiles of SF_6 from stations 75 km north, south, east, and west of the tracer injection site (Figure 1). The bar indicates ± 1 standard deviation of analysis.

concentration and the rms error of analysis were approximately 0.04 fM. The results for the northern cast may have been falsely elevated by the presence of personnel who had recently transferred from *Oceanus* after participating in the tracer release, however.

3.4. Initial Survey

Sampling of the initial patch commenced on May 14, 1992, 37 hours after the end of the injection, and continued to May 31, from RRS *Charles Darwin*. A special sampling system had been developed to overcome streakiness anticipated in the initial patch. An array of 18 to 20 integrating samplers was deployed along the cable at spacings of 2 to 6 m (Figure 6). Four auxiliary CTDs (Sea-Bird Sea-Cats) were interspersed in this array. At the center of the array was a sled containing 2 integrating samplers, an 18-syringe sampler, an EG&G Mark-III CTD, and a rosette of six Niskin bottles for salinity calibration.

The sampling array was tripped by mechanical messenger and towed at speeds of 0.3 to 1 m/s through the tracer patch for 3.5 hours at a time, while the integrating samplers continuously drew a total of 850 ml of water into a metalized bag. The 18 glass syringes at the CTD filled sequentially along the tow track, each taking 11 min to obtain 60 mL of sample, with a 24-sec gap between samples. They were driven by a hydraulic system triggered from the rosette. Thus, while the integrating samplers gave a set of samples at various heights above the CTD, each sample being the integral along a path 6 to 12 km long, the 18-chamber sampler gave a sequence of samples at the CTD, each one being an integral over 200 to 600 m of the track. Neither sampling device worked perfectly. The integrating samplers tended to fill faster toward the beginning and to slow down or even to stop later in their fill period. The syringe samplers would often fill only partially, or not at all. For some casts the entire syringe system failed to start.

The CTD was held as close as possible to the target density surface by an automatic control system similar to that used for the injection. The rms variation of potential density at the CTD was less than 0.003 kg/m^3 for most of the tows, equivalent to less than 2 m rms displacement. The samplers along the wire collected water of a greater variety of densities mostly because of the strain associated with internal waves and fine structure. The purpose of the auxiliary CTDs along the wire was to quantify this variability and therefore to help estimate the initial diapycnal distribution of the tracer.

The bag samples from the integrating samplers were transferred to syringes and analyzed by head-space anal-

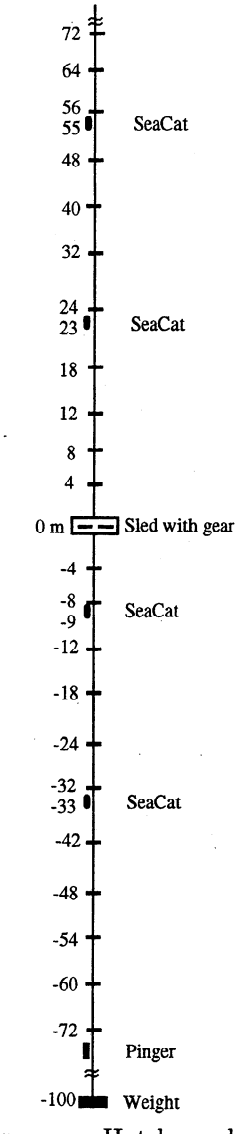

Figure 6. Sampler array. Hatch marks indicate integrating samplers.

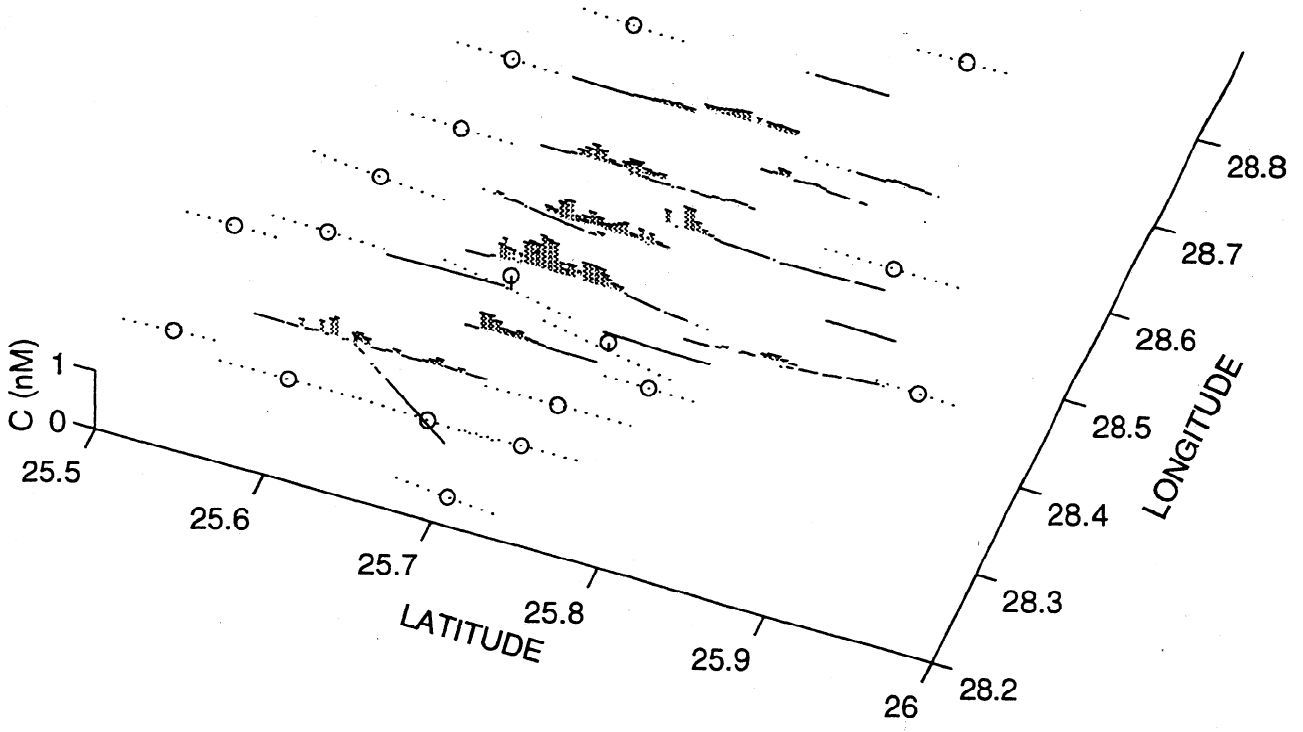

Figure 7. Initial tracer survey viewed from the northeast. The heights of the "fences" show the concentrations from the multichamber sampler. Where these concentrations were very low, a solid line appears along the tow tracks. Dotted line segments with circles in the middle show tows for which little or no tracer was found. The two dotted line segments near the middle of the patch with circles raised above the track are cases for which the multichamber sampler malfunctioned, the height of the circle indicating the concentration in the central integrating sampler.

ysis [*Law et al.*, 1994]. The inner surface of the bags retained approximately 6% of the SF_6 from the water. Flushing of the bags with nitrogen after each sample avoided contamination of subsequent samples. Samples from the hydraulically driven syringes were also transferred to normal glass syringes for head-space analysis. The rms error in SF_6 concentration for the bag samples is estimated as less than 2%, while that for the syringe samples was 2 to 5%.

The 42 tow tracks occupied during the survey are shown in Figure 7, where an adjustment has been made for advection during the survey based on float positions obtained with short-range acoustics. The float data indicate a fairly uniform velocity to the west of about 1 cm/s for most of the patch. However, a float released early in the injection with the westernmost streak moved much faster to the west, with a mean speed of nearly 6 cm/s. Thus there appeared to be a positive zonal strain within the patch. The tracks shown in Figure 7 have been translated to positions estimated for May 23, 1992. The 16-day survey was far from synoptic, so the uncertainty in these translations is large.

Figure 7 also depicts most of the raw data pertinent to the lateral distribution of the tracer at the time of this first survey. Included are individual syringe concentrations where available, and the integrating sampler concentration at the target density surface otherwise. Figure 7 suggests that the injection streaks had formed a nearly continuous patch that had been stretched zonally and compressed meridionally by a factor of two or so by the strain field.

The spacing of the sampling tracks is too great to make a very detailed map of the tracer distribution. However, a smoothed map (Figure 8) can be made with the method described in the appendix. The total amount of tracer found within the error contour shown in Figure 8 is 993 $\pm$ 80 moles, compared with 951 moles injected. Some surplus could be due to smoothing by the mapping technique and to nonsynopticity of the survey. On the other hand, it is possible for tracer to have escaped to the west or the northeast. The rms dispersion in the zonal and meridional directions estimated from the map were 7.5 and 5.1 km, respectively (Table 1).

The vertical profiles of tracer concentration for the initial survey from the integrating samplers show a variety of peak shapes, with maxima generally within a few meters of the target density surface, and with rms widths of the order of 5 m. Figure 9 shows some of the 28 profiles obtained. Uncertainties in the mean profile (Figure 10) are calculated from the variance in the shapes of the individual profiles, as in the work of *Led-*

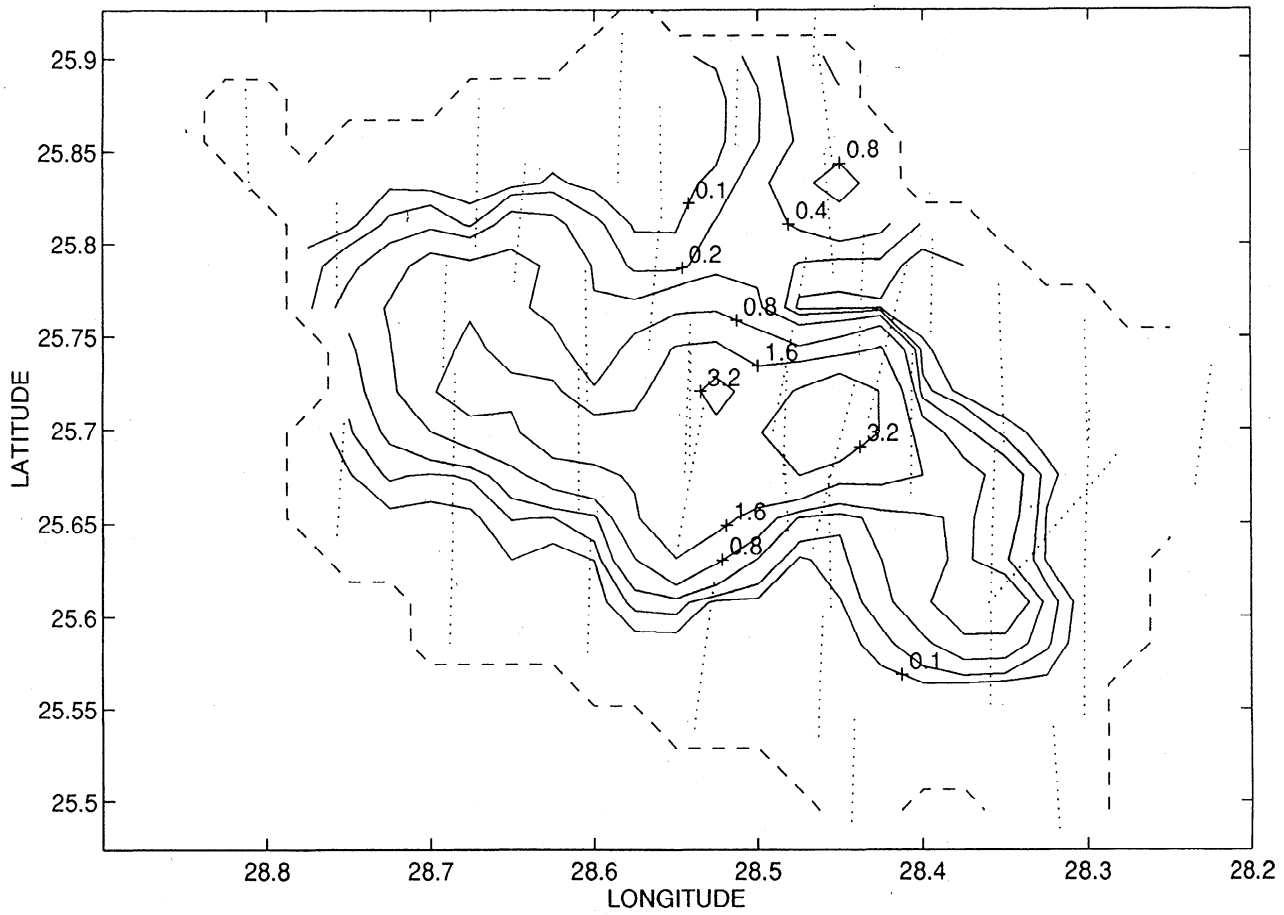

Figure 8. Smoothed map of the initial tracer patch. The column integral is contoured in units of 10^{-6} mol/m^2. The dashed line delimits the area used to estimate moments, based on the uncertainty of the map.

well and Bratkovich, [1995]. The mean profile is slightly small in the shoulders and high in the tails compared with a Gaussian. This shape is expected for a profile that is Gaussian in density space but distorted by towing at constant heights through the strain field of the internal waves [*Ledwell and Watson*, 1991]. The temperature variance at the auxiliary CTDs deployed along the wire enable corrections to be estimated for towing through the strain field if it is assumed that the strain is uncorrelated with fluctuations in the distribution of tracer with density. The dotted profile in Figure 10 shows a Gaussian profile which, when distorted by towing through the strain field, gives the best fit (dashed profile) to the observations. This profile is a better estimate of the initial condition than the measured profile, although the difference is of consequence only to the evaluation of the injection.

3.5. October 1992 Survey

The second survey of the tracer was performed from R/V *Oceanus* during October 1992. The sampling apparatus was the same one used for the initial survey, with the following changes. The 18-syringe sampler was replaced by a 50-syringe sampler. The spacing of the integrating samplers was approximately doubled to accommodate the increased vertical spread of the patch. The tow speed was increased to a little over 1 m/s, and the tow time was increased to 7.5 hours to accommodate the larger area occupied by the tracer. Thus the length of the tow tracks was approximately 30 km, and the resolution of the 50-syringe sampler was approximately 600 m. Also, the 5-L Niskin bottles on which the integrating samplers were mounted were used to obtain spot samples for comparison with the integrated samples.

A west-southwest drift of the patch of about 1 cm/s was anticipated from historical data [*Armi and Stommel*, 1983; *Bauer and Siedler*, 1988; *Thiele et al.*, 1986], and from the path of a neutrally buoyant float that was about 100 km north of the patch (provided by R. Davis). During the early part of the cruise, ranges to two of the floats deployed with the tracer were consistent with this estimate of the drift; one float was ~120 km southeast of the expected center of the patch, and the other was ~120 km southwest. A progressive vector diagram obtained later in the cruise from the current meters on

Table 1. Characteristics of the Lateral Distribution of the Patches

Survey	N, moles	X_{cm},° W	Y_{cm},° N	σ_x, km	σ_y, km	A_t, km^2	A_p, km^2
Injection	951 ± 34	28.27	25.67	7.5	5.1	6 (2 to 40)	400 (300 to 600)
May 1992	993 ± 80	28.52 ± .03	25.72 ± .02	10.7± 3.6	6.7 ± 2.9	400 ± 100	680 ± 100
Fall 1992	300 ± 70	–	–	–	–	2 x10^4 (1.3 to 3.3)	1.5 x 10^5 (1 to 4)
Spring 1993	897 ± 28	32.2 ± 1.0	25.0 ± 0.8	230 ± 65	140 ± 40	(3.5 ± 1) x 10^5	(5 ± 1) x 10^5
Nov. 1994	–	37.6 ± 1.5	22.3 ± 3.0	510 ± 130	290 ± 70	(3 ± 1) x 10^6	(3 ± 1) x 10^6

the central mooring indicated a mean drift of about 1 cm/s, slightly north of west.

The tracer was found by towing along a continuous line, starting near 24°10'N, 29° 50'W, 100 km south of the expected center of the patch. A strong streak of tracer was encountered after 150 km of track was occupied (Figure 11; the tracer shown for November was not encountered in October where the ship track crosses it). After determining that this streak was isolated, a strategy was devised to cross it repeatedly while moving along its length. An apparently continuous streak about 300 km long was revealed (Figure 11). The segment of the streak first found seemed well defined, with an rms width of about 3 km. The streak broadened into a less well defined patch some 40 km across in the northeast, where the concentrations were high. Another such patch with lower concentration was observed at the western end (Figures 11 and 12). The amount of tracer found on this survey is estimated to be approximately 18% of the total injected.

Profiles from the integrating samplers revealed a vertical distribution about three times broader than found during the initial survey (Figure 13). Again, there are interesting variations in detail among profiles, but most are strongly and singly peaked within 10 m of the target density surface. Profiles from samples taken with Niskin bottles were surprisingly similar to those from the integrating samplers (Figure 14), indicating that there was no huge variance of concentration or profile shape within the streaks even if examined with spot samples.

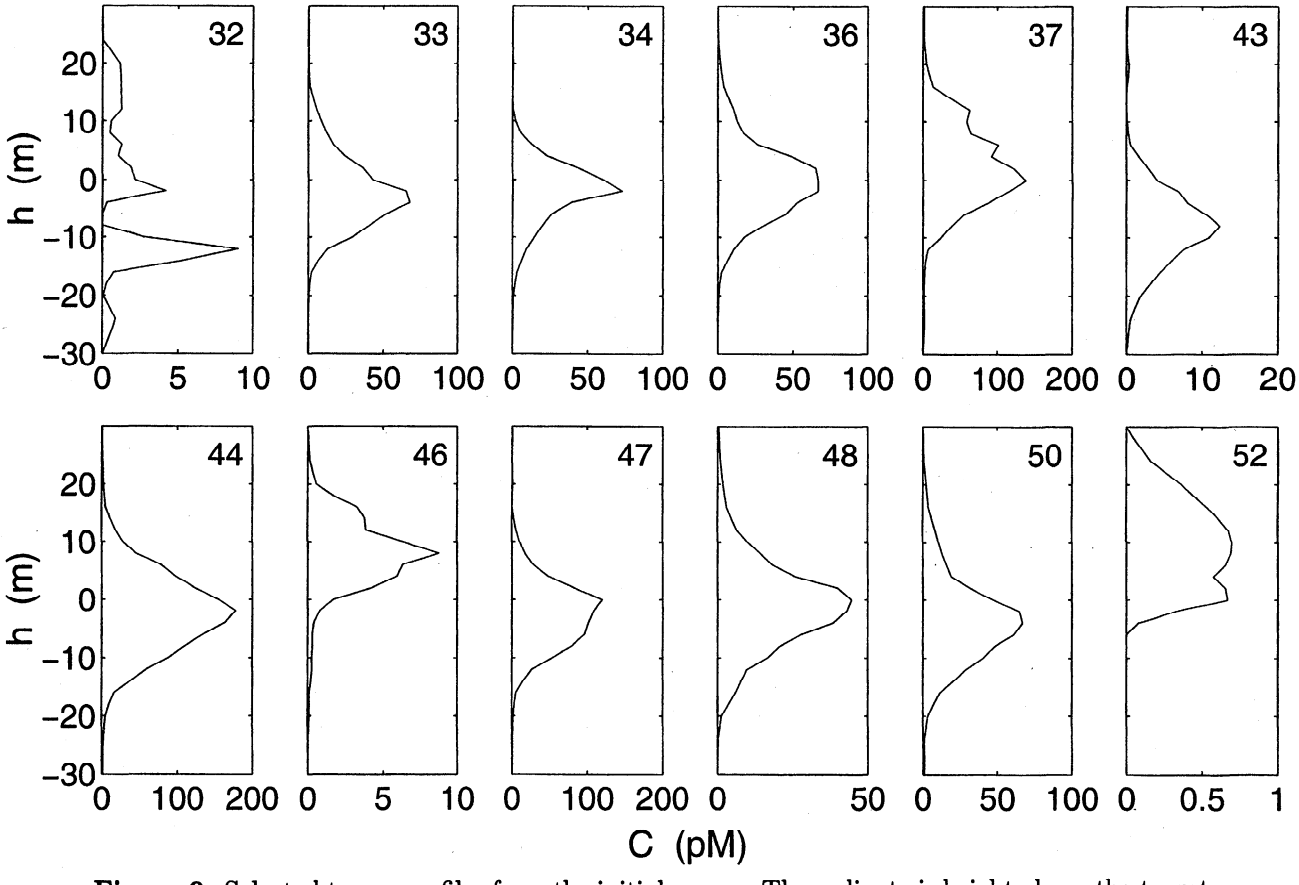

Figure 9. Selected tracer profiles from the initial survey. The ordinate is height above the target density surface. Note changes in the abscissa scales.

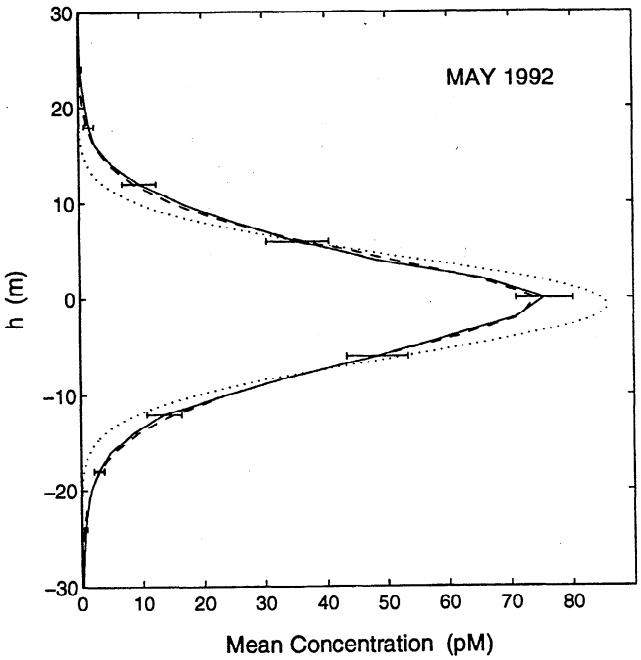

Figure 10. Mean tracer profile from the initial survey (solid line with error bars). Height h is relative to the target density surface. The dotted curve is the Gaussian curve that would be distorted into the best-fit dashed curve by towing through the observed strain field (see text).

The mean of the 22 profiles from the integrating samplers yielded a profile which was fit well by a Gaussian with center of mass 3.4 ± 1.5 m below the target density surface (Figure 15). Again, the actual profile is estimated with account taken of towing through the strain field.

3.6. November 1992 Survey

Sampling continued from R/V *Oceanus* between October 26 and November 19, 1992, with conventional rosette casts, spot samples having proved promising. Stations were spaced 9 km apart and occupied approximately every 6 hours. A companion program by N. Oakey and colleagues obtained microstructure data between stations [*Ruddick et al.*, 1997]. What seemed to be the southeastern end of the streak from the previous cruise was found and followed for another 250 km to the southwest (Figure 11). The streak appeared to be continuous, even at the coarse sampling resolution of 9 km. Individual vertical profiles were similar to those found on the prior cruise (Figure 16). The mean profile was again quite Gaussian (Figure 17). Because discrete samples were taken, no uncertainty enters from towing, but a transformation between potential density and depth must be made. The ordinate in Figure 17 is the potential density, transformed to height above the target density surface with the mean vertical density profile for the survey. The first moment of the Gaussian fit to the November profile was 5.6 ± 1.5 m below the target density surface.

The total amount of tracer accounted for on the November cruise was approximately 15% of that injected, bringing the total for the two fall 1992 surveys to 33%. This estimate assumes that none of the tracer sampled in November had not already been sampled in October. Float trajectories for the time period indicate that it is possible that the patch at the northeast end of the October survey had indeed moved to the south, suggesting that there was some resampling of tracer. Hence, at least two thirds of the tracer injected was not found during the fall of 1992. There must have been more streaks or patches outside the region sampled. Available float trajectories suggest that the streaks that were found might extend to the west and that there may be tracer to the southeast, as suggested by the unclosed limb near 24°30'N, 29°00'W in Figure 11. However, the float trajectories do not point to a region where there might have been a rich lode of unsampled tracer.

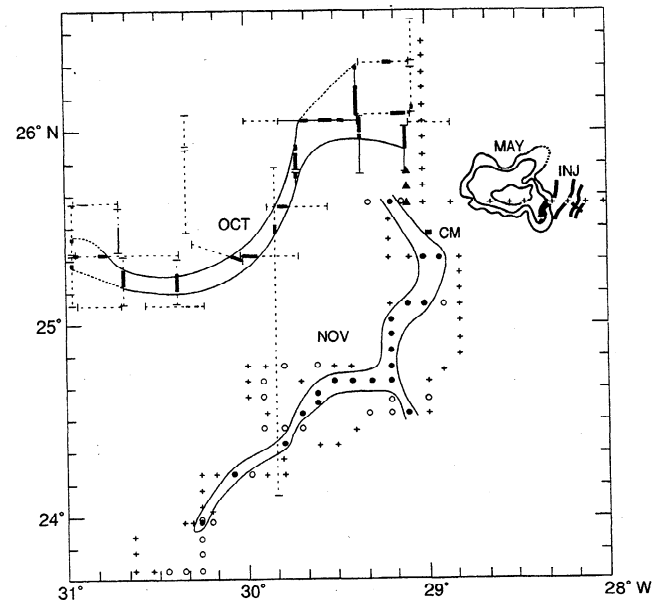

Figure 11. Lateral distribution of tracer found in the fall of 1992. Injection streaks are shown as short heavy lines near 26°N, 28°W. Closed contours just to the west show the patch in May 1992. Heavy lines further to the west show track segments for the October survey on which the concentration C at the target surface was greater than 500 fM; light solid lines show where C was between 100 and 500 fM; dashed lines show where C was much less than 100 fM. Solid triangles indicate bottle stations occupied at the end of the October cruise, with $C > 300$ fM. Station symbols for the November survey are: plus, $C < 30$ fM; open circles, $C = 30$-300 fM; solid circle, $C > 300$ fM. A fine curve has been drawn to envelop the high concentration regions for the two surveys. CM Marks the location of the central mooring for the Subduction Experiment. *Ledwell et al.* [1993], reprinted by permission from *Nature*, vol. 364, p. 701, copyright 1993 MacMillan Magzaines Ltd.

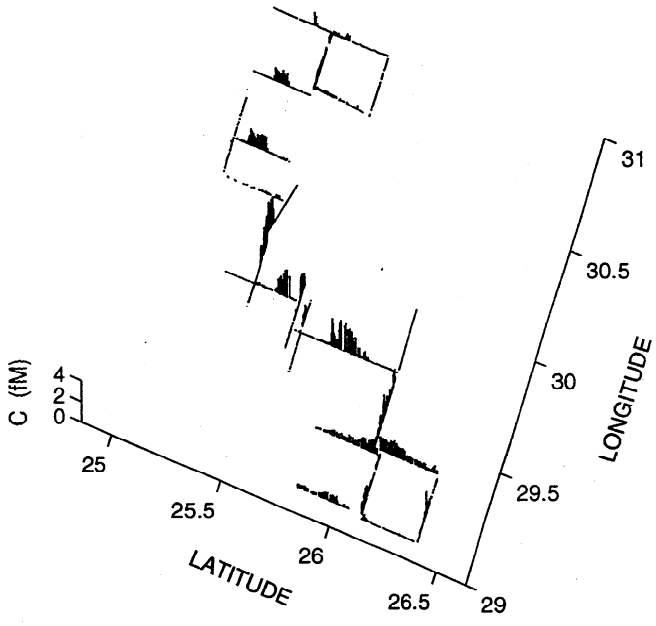

Figure 12. Tracer distribution for October 1992 viewed from a high angle in the northeast. Concentrations are indicated by the heights of the line segments along the tow tracks. Where the concentrations were low, only a solid line along the tow track appears.

3.7. Spring 1993 Survey

CSS *Hudson* and RRS *Charles Darwin* returned to sample the patch in April and May 1993 with discrete water samples. Tracer was found on nearly every cast within a broad area (Figure 18), in striking contrast to the experience 6 months before, when most of the region surveyed was free of tracer. Apparently, the streaks of tracer had grown so much that they had painted the region nearly completely, as anticipated by *Garrett* [1983] and *Haidvogel and Keffer* [1984]. Still, there was a great deal of structure at the resolution of the survey, which was typically 20 km along the tracks, and 111 km between tracks.

A smoothed map (Figure 19) can again be made with the method described in the appendix. The total amount of tracer within the error contour shown on the map is 897 ± 28 moles, compared with 951 moles injected. The map shows that it is likely that some tracer lay beyond the error contour to the north and northwest. Other integral properties of the patch are listed in Table 1 and are discussed in section 6.

While considerable variation among individual vertical profiles remained (Figure 20), only a dozen profiles or so are required to obtain a stable estimate of

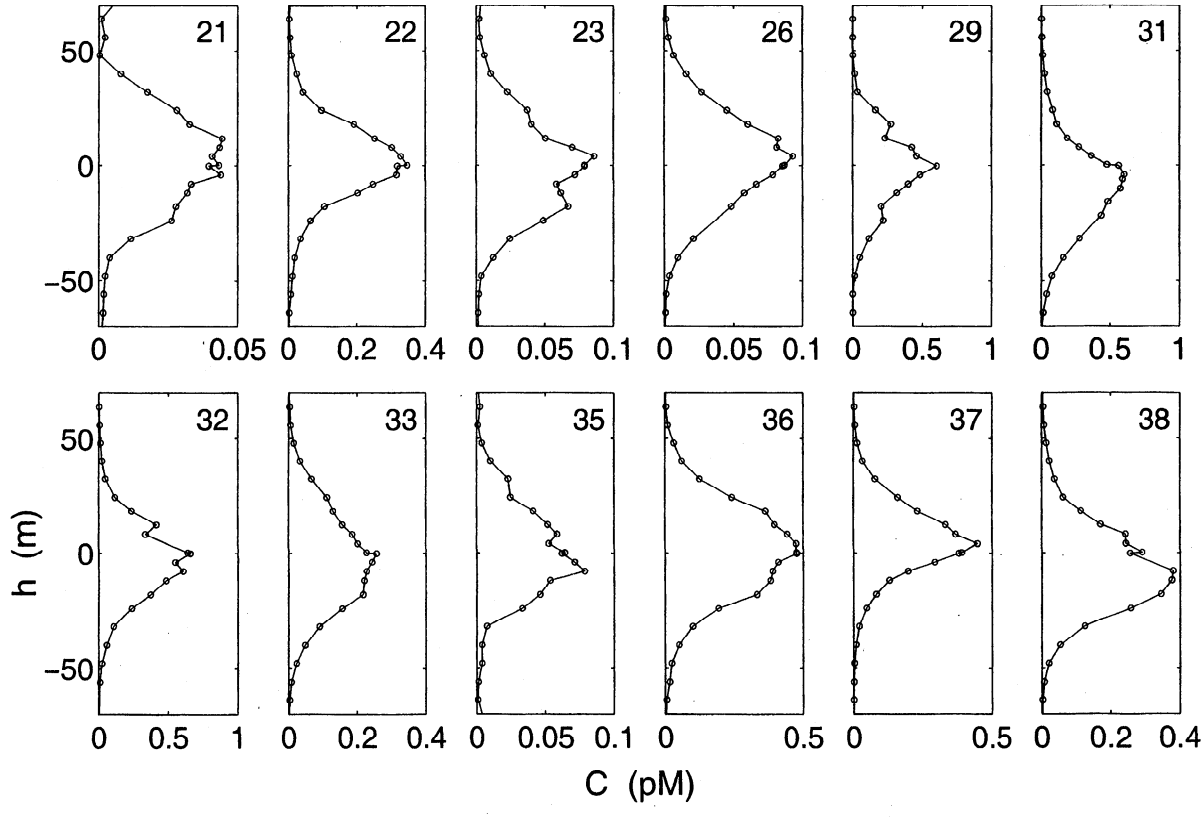

Figure 13. Selected tracer profiles from the integrating samplers, October 1992. Axes are defined as in Figure 9. Note changes in the abscissa scales.

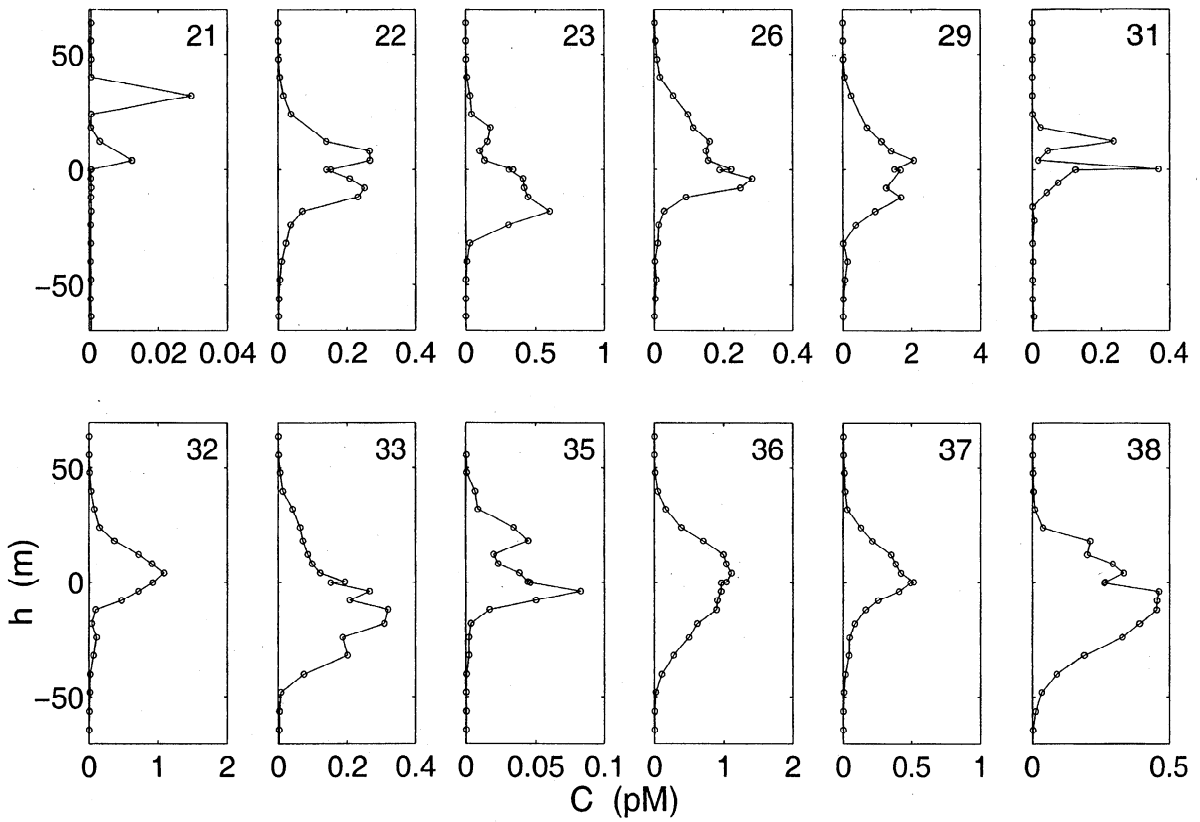

Figure 14. Selected tracer profiles from the Niskin bottles, October 1992. Axes are defined as in Figure 9.

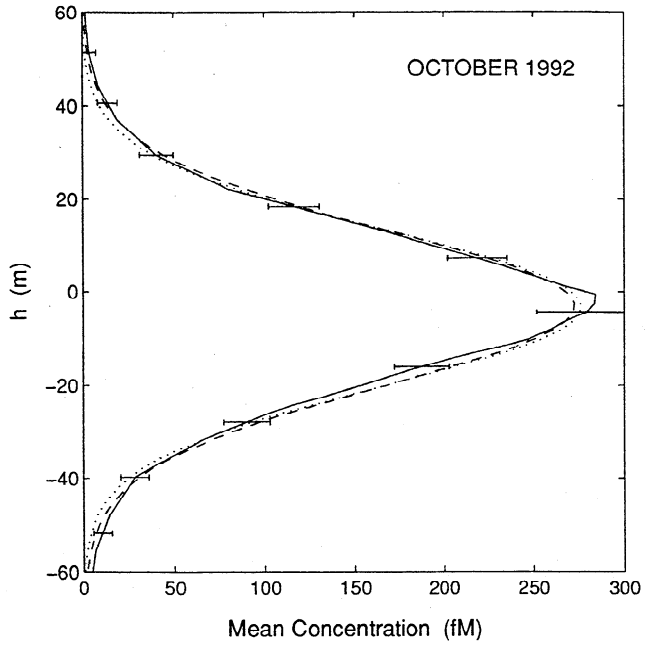

Figure 15. Mean tracer profile from integrating samplers, October 1992. The various curves are defined as in Figure 10.

mean concentration versus density. To show this, the 165 stations occupied by RRS *Charles Darwin* which found tracer were divided by geographical area within the patch into groups of 6 to 19, and a mean profile was calculated for each group. The second moments of Gaussian fits to these mean profiles vary little with location (Figure 21). The diapycnal distribution of the patch seems to have been greatly over sampled. The overall mean profile is very close to a Gaussian with first moment 5.6 $\pm$ 1.0 m below the target density surface (Figure 22).

3.8. November 1994 Survey

The western part of the patch was sampled from R/V *Seward Johnson* in November 1994, 30 months after injection. A series of rosette stations approximately 100 km apart found a smoother patch than had been found at 12 months (Figure 23). Analysis of spatial variability and speculation of how the patch extends to the east are left to section 6.

The vertical profiles (Figure 24) from this survey were more similar to one another than for earlier surveys and, as for the spring 1993 surveys, revealed no clear trends

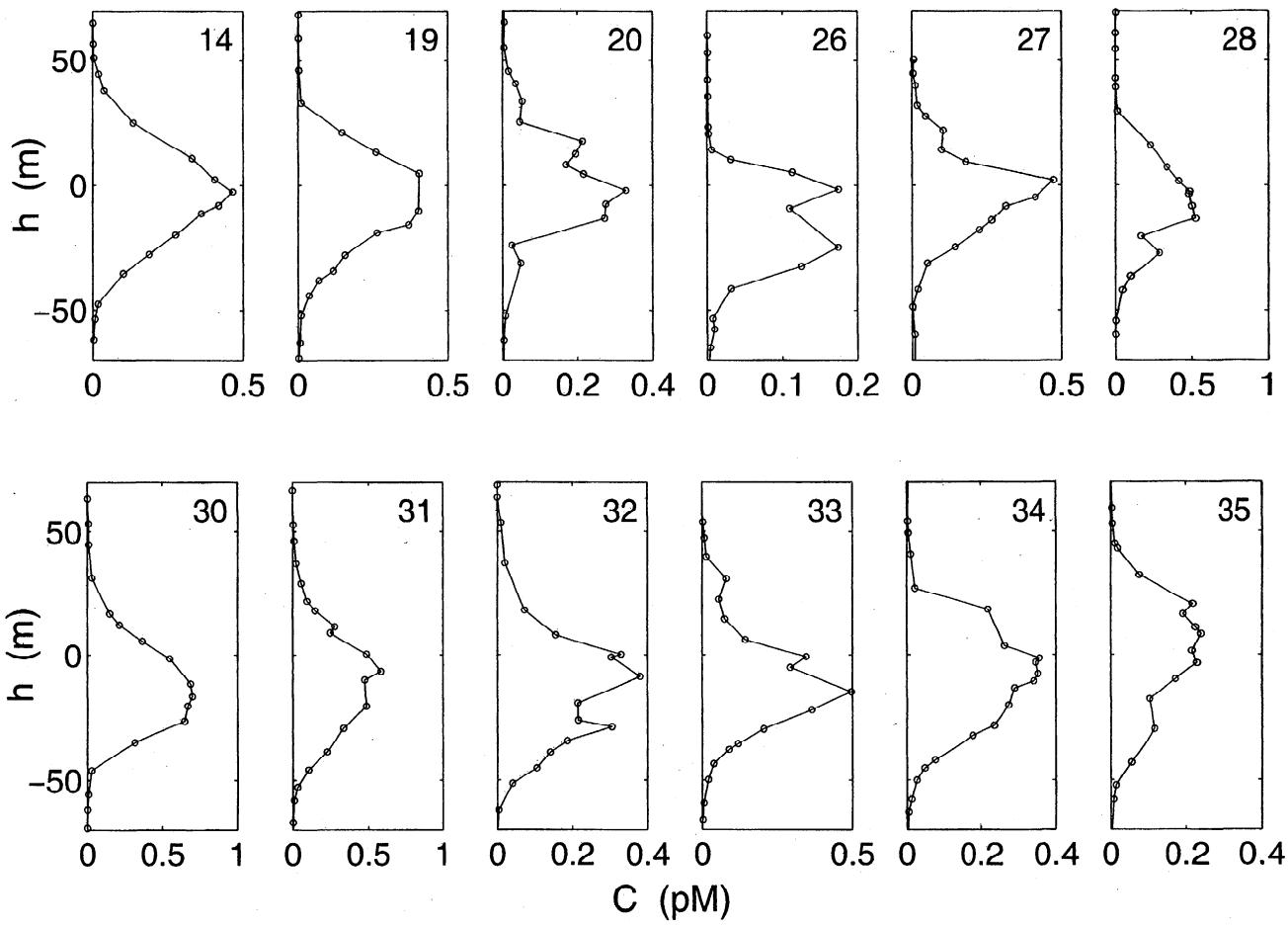

Figure 16. Selected tracer profiles from rosette sampler, November 1992. Axes are defined as in Figure 9.

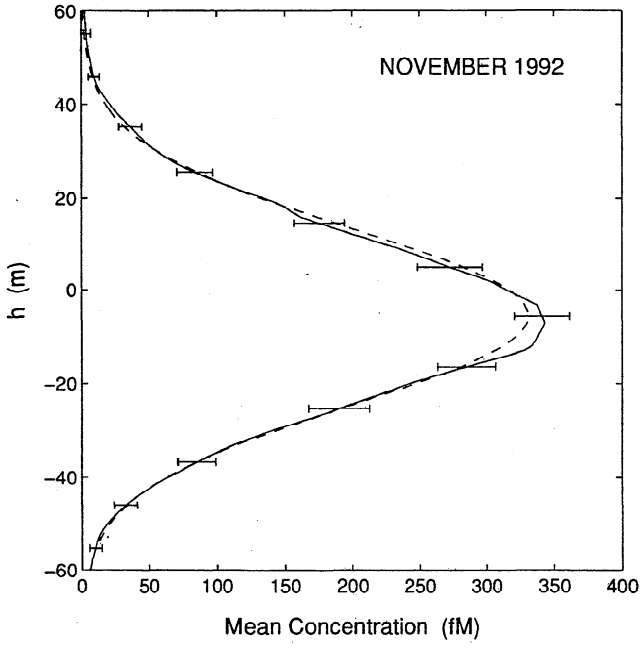

Figure 17. Mean vertical profile for November 1992 (solid curve) and the best fit Gaussian (dashed curve).

in their first or second moments with position. The mean profile was again quite close to a Gaussian, even though it spanned more than 200 m of the water column (Figure 25). The center of mass had descended to 8 m below the target density surface. Peak tracer concentrations had by this time fallen to 10 fM, around 20 times background, so uncertainties in the background may contribute systematic errors, especially in the tails. A correction to the background measured in 1992 (Figure 5), which increases linearly with height h above the target density surface from 0 fM at h = -200 m to 0.08 fM at h = 200 m, has been subtracted from the mean profile to bring the upper tail to zero in Figure 25. Uncertainty assigned in the upper tail of the mean profile has been increased accordingly in the model runs discussed in the next section.

4. Diapycnal Diffusivity

The nearly Gaussian shape of the tracer distribution for each survey, with ever increasing width, shows that the evolution of the distribution is governed approximately by the diffusion equation, and suggests that

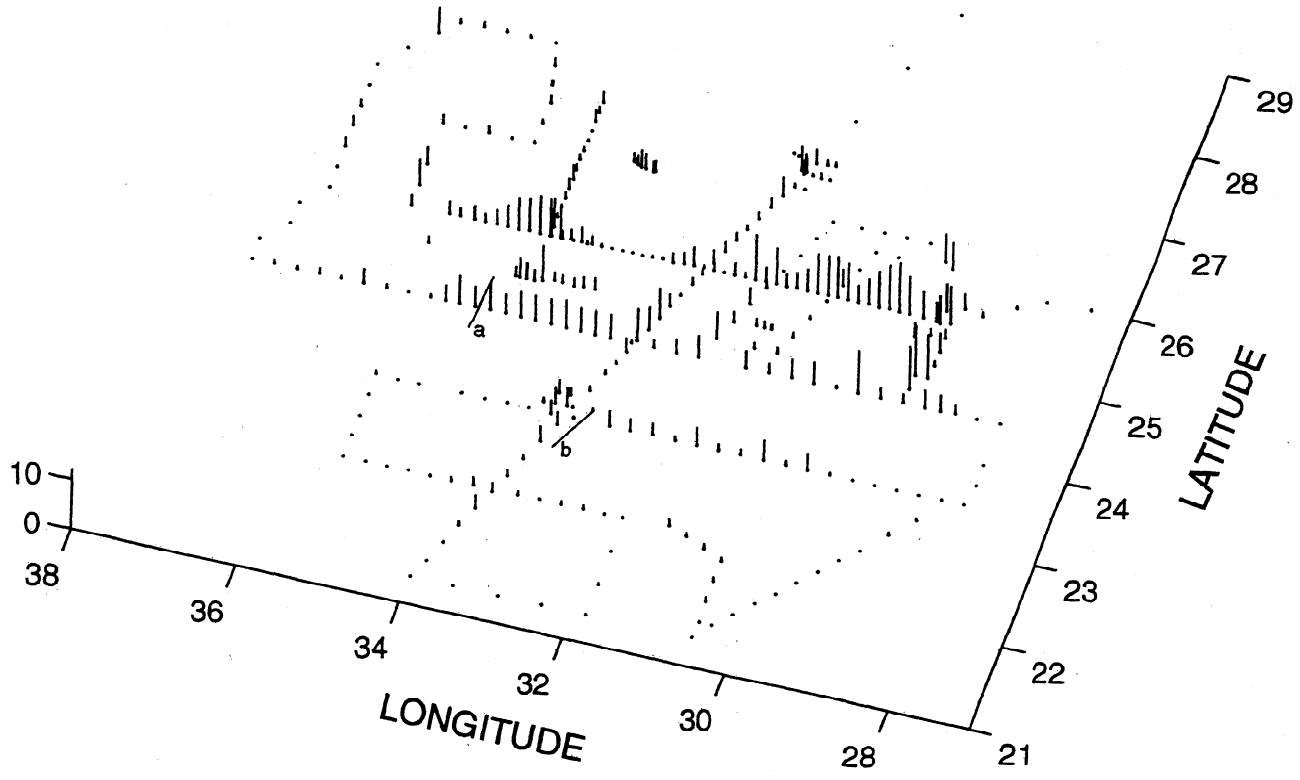

Figure 18. Tracer distribution in spring 1993, viewed from the southeast. The height of the vertical lines represents the column integral of tracer, in nmol/m^2. Stations where no tracer was found appear as dots. The lines marked *a* and *b* show the tracks for the multichamber results shown in Figures 30a and 30b.

the diapycnal diffusivity can be estimated fairly directly from the time series of the widths. Rather than do this, however, we have fit the data to a more elaborate version of the advection-diffusion equation which allows exploration of the sinking of the tracer relative to the target surface and brings out important sources of uncertainty.

The advection-diffusion equation is

$$\frac{\partial c}{\partial t} + \mathbf{u} \cdot \nabla c = D \, \nabla^2 \, c \tag{2}$$

where c is the tracer concentration, $\mathbf{u}$ is the velocity, and D is the molecular diffusivity.

Now average (2) over a region of area A, independent of depth, which encompasses all of the tracer. At the boundaries of this region the concentration is zero. Application of Gauss' theorem in two dimensions and invocation of the continuity equation gives

$$\frac{\partial \overline{c}}{\partial t} + \frac{\partial (\overline{wc})}{\partial z} = D \, \frac{\partial^2 \overline{c}}{\partial z^2} \tag{3}$$

where the overbar represents the area average.

The coordinate z is normal to smoothed isopycnal surfaces, which are taken to remain parallel to one another in the region of the patch, although they may converge with time following the patch. This approximation amounts to ignoring effects due to the covariance of the concentration profile with layer thickness. It is justified by Figure 21, which shows very small regional variation in the concentration profiles.

We decompose $\overline{wc}$ into a mean part and an eddy part, through which we introduce the diffusivity K:

$$\overline{wc} = \overline{w} \, \overline{c} - K \, \frac{\partial \overline{c}}{\partial z} \tag{4}$$

Using (4) in (3), and folding D into K, we have

$$\frac{\partial \overline{c}}{\partial t} + \left(\overline{w} - \frac{\partial K}{\partial z} \right) \frac{\partial \overline{c}}{\partial z} + \frac{\partial \overline{w}}{\partial z} \, \overline{c} = K \, \frac{\partial^2 \overline{c}}{\partial z^2} \tag{5}$$

The data are analyzed as a function of height h above the target density surface at potential density anomaly $\sigma = \sigma_o$, so we make the transformation:

$$\begin{aligned} h &= z - z(\sigma_o) \\ \left(\frac{\partial}{\partial t} \right)_z &= \left(\frac{\partial}{\partial t} \right)_h - \left(\frac{\partial z}{\partial t} \right)_{\sigma_o} \left(\frac{\partial}{\partial h} \right)_t \\ \left(\frac{\partial}{\partial z} \right)_t &= \left(\frac{\partial}{\partial h} \right)_t \\ \overline{w} &= \left(\frac{\partial \overline{z}}{\partial t} \right)_\sigma + \overline{w}_d \\ \overline{w}_d &\equiv \left(\frac{\partial \overline{z}}{\partial \sigma} \right)_t \frac{d\overline{\sigma}}{dt} \end{aligned} \tag{6}$$

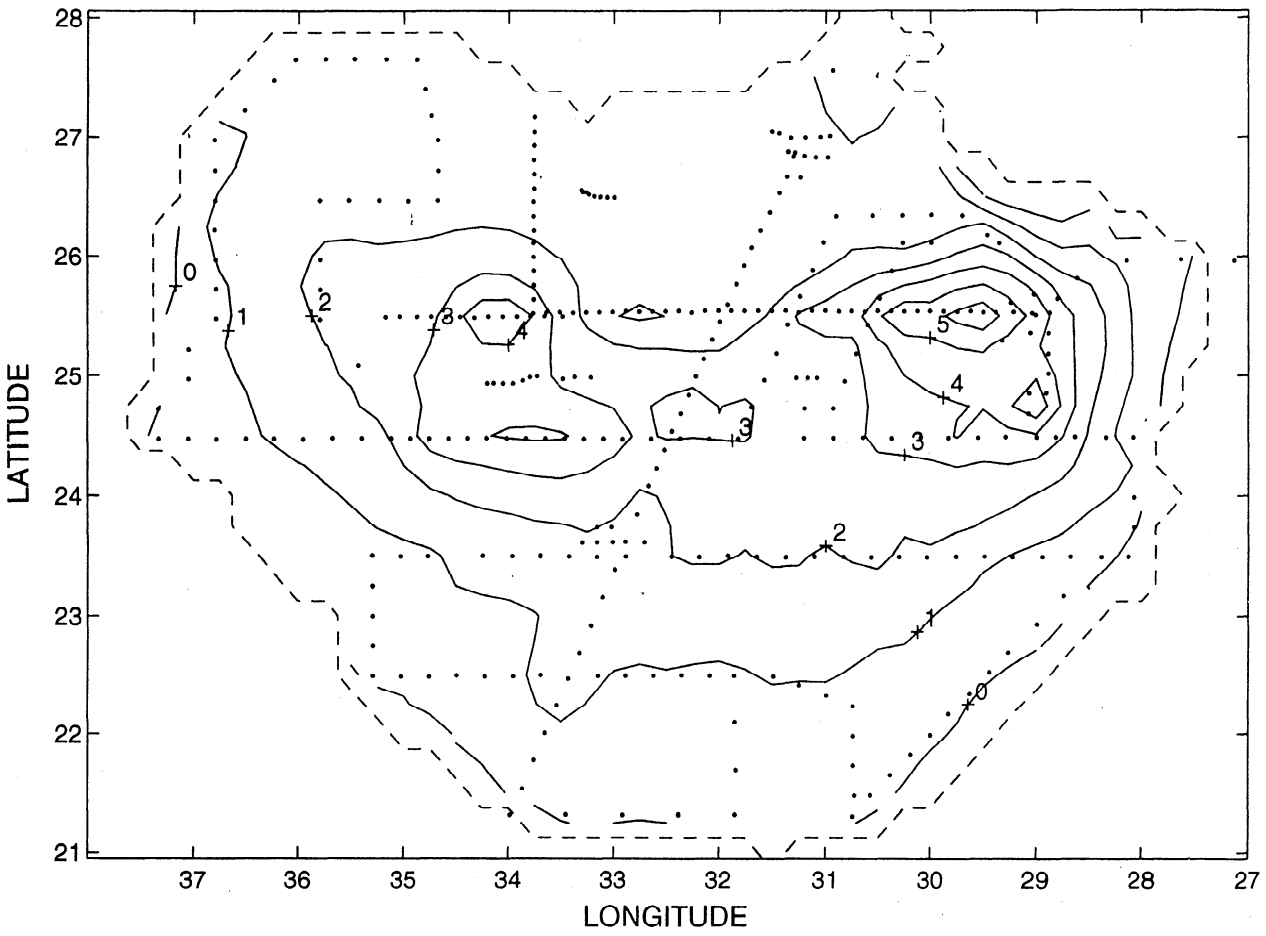

Figure 19. Column integral of SF_6, contoured at intervals of 1 nmol/m^2 for spring 1993. The dashed curve delimits the region within which area integrals are estimated.

Here $(\partial\overline{z}/\partial t)_\sigma$ is the normal velocity of the isopycnal surfaces, and $\overline{w}_d$ is the mean velocity of tracer through the isopycnal surfaces. The $d\overline{\sigma}/dt$ is the average time derivative of potential density following tracer. It is due to changes in potential density of the water by mixing processes, both diapycnal and isopycnal, and may also have a contribution from transport on sinking particles. Because of the variety of possible contributions to $\overline{w}_d$, it is not possible here to express it as a function of K through the density equation. This would be true even in the absence of particle transport because the diapycnal diffusivity for heat is most likely not the same as for salt and tracer (see section 5 below), and because cabbeling by isopycnal mixing must be considered.

Using (6) to transform (5), we have

$$\frac{\partial\overline{c}}{\partial t}+\left(\overline{w}_d-\frac{\partial K}{\partial h}\right)\frac{\partial\overline{c}}{\partial h}+\frac{\partial}{\partial h}\left[\left(\frac{\partial h}{\partial t}\right)_\sigma\overline{c}\right]=K\frac{\partial^2\overline{c}}{\partial h^2} \quad (7)$$

where we have taken $\overline{w}_d$ to be independent of h, i.e., the diapycnal velocity, whatever its cause, is approximated as being nondivergent.

The quantity $(\partial h/\partial t)_\sigma$ represents the vertical movement of isopycnal surfaces relative to the target density surface from survey to survey (Figure 26). Since $\overline{w}_d$ is taken as independent of h, this movement is constrained to be adiabatic, i.e., as due to the divergence of water out of the tracer patch. This divergence in the tracer layer is about twice that required to conserve planetary potential vorticity as the patch moves south. A careful analysis of the uncertainty and implications of this observation has not yet been undertaken.

The evolution of the tracer distribution has been modelled with (7) using the least squares methods described by *Ledwell and Watson* [1991] and *Ledwell and Bratkovich* [1995] to find K, $\partial K/\partial h$, and w_d simultaneously. The experiment is divided into three periods, with the surveys as endpoints. The estimates indicate that the diffusivity felt by the tracer increased from 0.12 cm^2/s for the first 6 months to approximately 0.17 cm^2/s for the remaining 24 months (Table 2). Since the area sampled by the tracer for the first 6 months was relatively small, the overall time- and area-weighted diffusivity is 0.17 cm^2/s. This estimate applies to the region between 30° and 45°W and between 20° and 25°N at the target potential density surface.

The uncertainties listed in Table 2 represent attempts

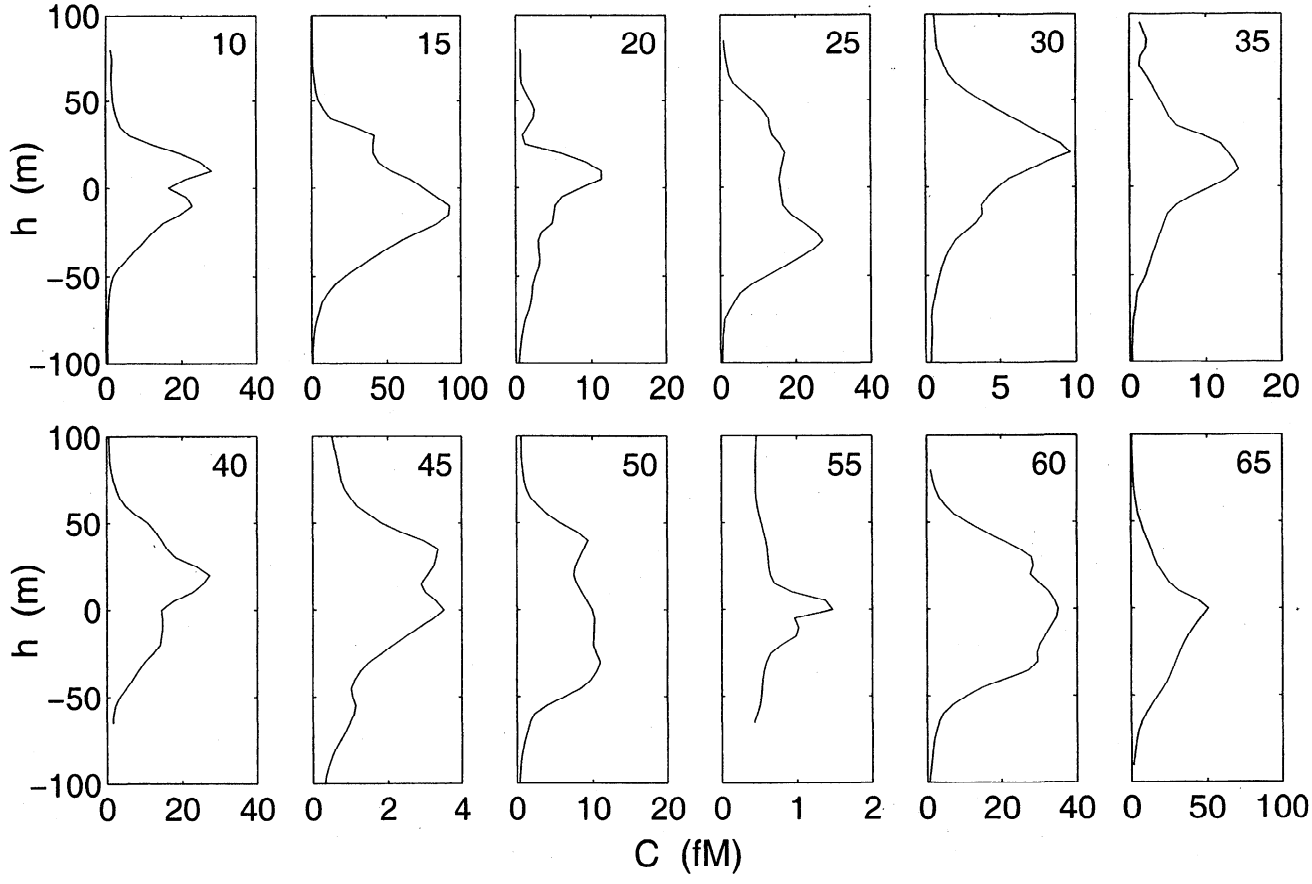

Figure 20. Selected tracer profiles from the spring 1993 survey. Axes are defined as in Figure 9. The background has not been subtracted.

to estimate 95% confidence intervals. These uncertainties arise from several sources, whose relative importance varies from one period to another. Most significant are the observed variations in the density profile $h(\sigma)$ already mentioned (Figure 26). Sampling error affecting the shapes of the mean profiles contribute significantly to each estimate as well. Uncertainties in accounting for towing through the fine-structure contribute to the estimates involving the May 1992 and October 1992 profiles but only mildly. Potential distortions due to persistent vertical shear can affect each estimate, because incomplete surveys are involved. However, this source of uncertainty is minor compared with the others and is much less than might be expected from experience with tracer experiments done over periods of a few days. The reason is that the distorting effect of shears of a magnitude that can persist for several months are overwhelmed by the homogenizing effect of lateral dispersion. Last, uncertainty in the SF_6 background contributes modestly to the uncertainty for the period from 12 to 30 months.

It is not known why $K$was lower during the first 6 months of the experiment than later, but it is difficult to ascribe this result to partial sampling of the patch in the fall of 1992. It may be that the diapycnal distribution of parts of the patch which were not found was broader, but the diffusivity in the region of space and time sampled by that part of the tracer patch that was found has been accurately measured. The only process that can upset this accuracy is distortion of the patch by persistent shear, but shear would also move the center of mass of the observed tracer relative to the target isopycnal. The center of mass had indeed moved downwards by approximately 4 m between the May 1992 survey and the fall 1992 survey. The low-frequency (5 month) shear required to move a third of the patch down this much is of the order 2×10^{-4} s^{-1}, which is unrealistically large. However, even if the results were interpreted this way, only 16 m^2 would be added to the second moment and the best estimate of K would merely change from 0.115 to 0.122 cm^2/s . In fact, other explanations for the downward motion of the tracer are offered in section 6. We interpret the low value for K as accurate and indicative of the size of variations in diapycnal mixing that can be expected in the subtropical pycnocline, even after averaging over an area on the order of 10^4 km^2 and a time of 6 months.

In an effort to explain this low K during summer 1992, data from the current meter mooring in the vicinity of the tracer patch (Figure 11) were examined. A quantity that is accessible with the current meters and that seems to be proportional to the energy supply for

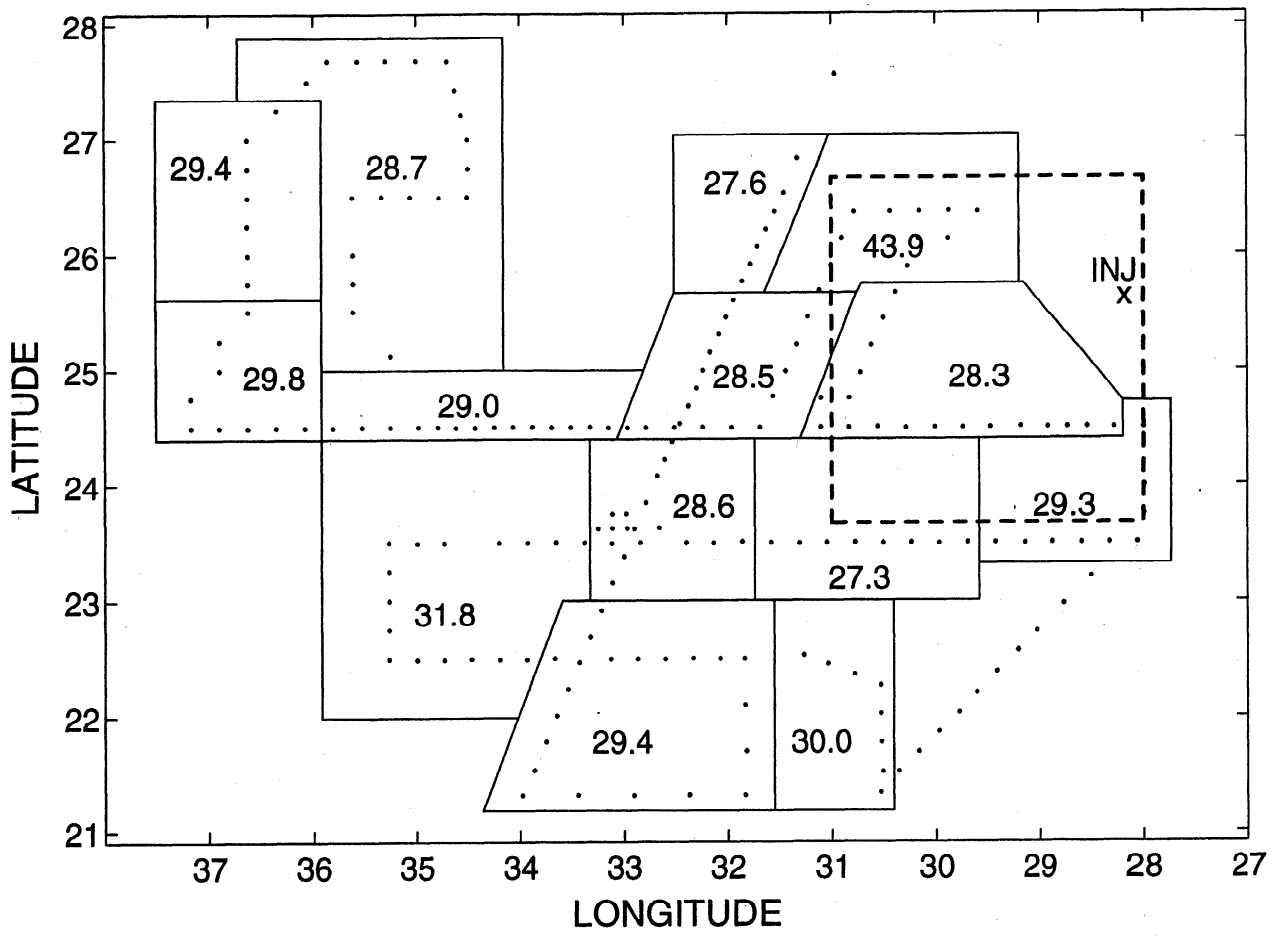

Figure 21. A map of the square root of the second moment of the mean tracer profile for geographical groupings of stations for spring 1993. The injection location (cross), and the frame of Figure 11 for the fall 1992 survey (dashed line) are shown.

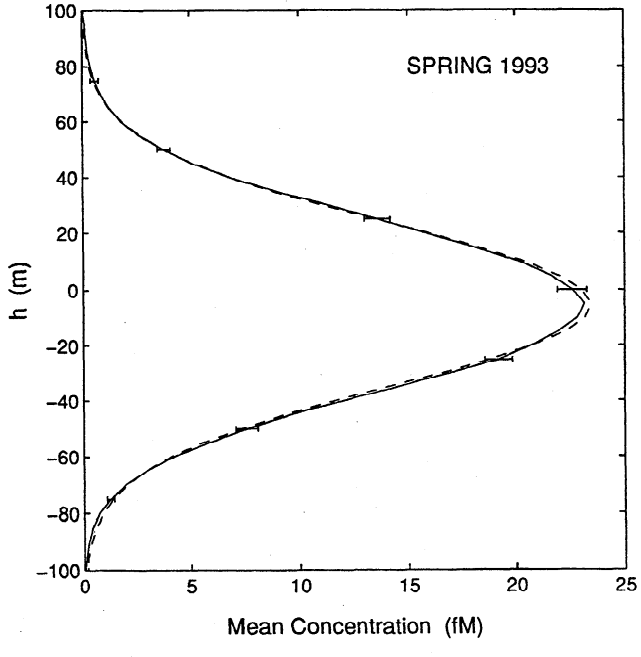

Figure 22. Mean tracer profile for spring 1993 (solid curve), and the best fit Gaussian (dashed curve).

diapycnal mixing from the internal wave field is the fourth power of the shear at 10-m separation S^4_{10} [*Gregg*, 1989; *Polzin et al.*, 1995a]. This quantity, calculated from the current meter data from 300 and 310 m depths, was very similar for the 8-month period after fall 1992 to that for the 6-month period before fall 1992 (Figure 27)

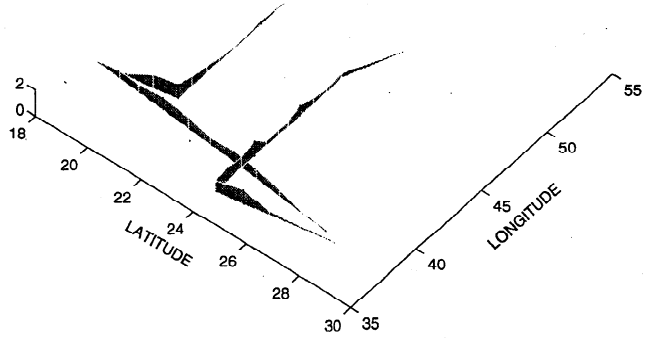

Figure 23. Tracer found in November 1994 viewed from the northeast. The height of the "fence" indicates the column integral, in nmol/m^2, with "posts" at the stations.

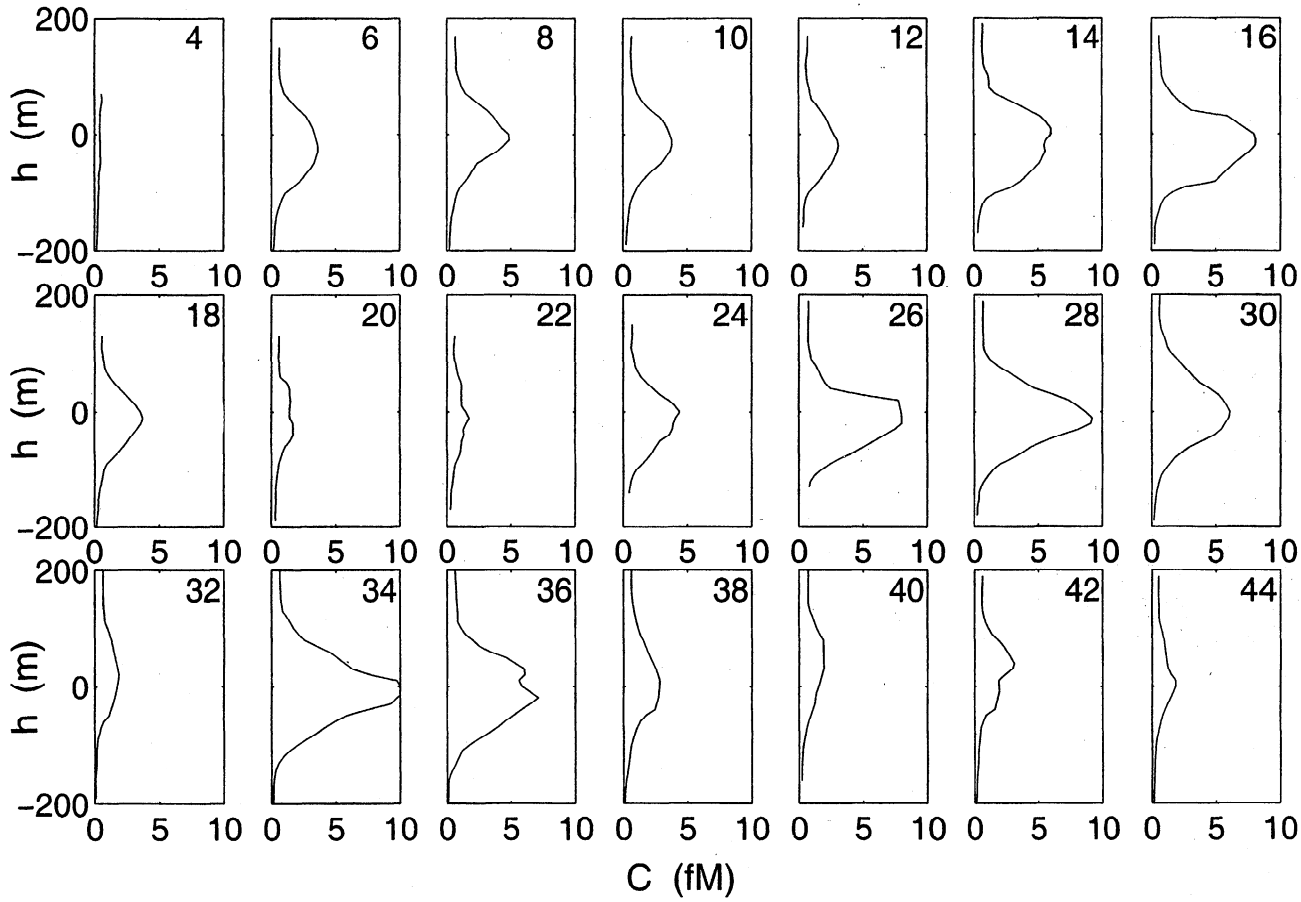

Figure 24. Tracer profiles for every other station from the November 1994 survey. Axes are defined as in Figure 9. The abscissa scales are all the same, and the background has not been subtracted.

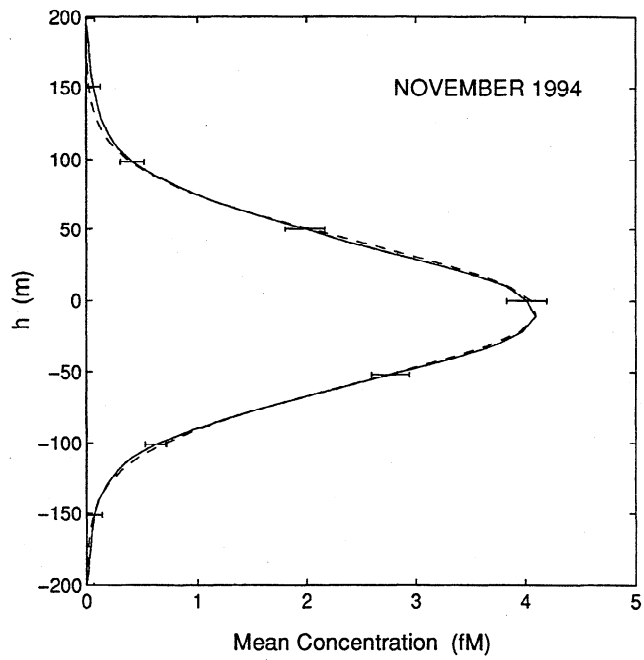

Figure 25. Mean tracer profile for November 1994 (solid curve), and best fit Gaussian (dashed curve). An ad hoc background correction of less than 0.1 fM has been applied to bring the upper tail close to zero (see text).

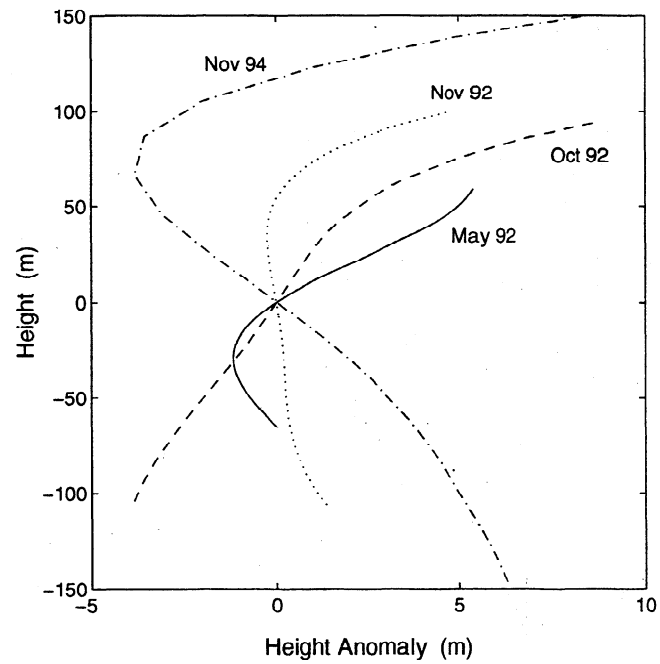

Figure 26. Mean heights of the isopycnal surfaces for various surveys above their mean height for the spring 1993 survey. The abscissa is the difference in height, while the ordinate is the height for spring 1993.

Table 2. Estimates of K

Period	K, cm^2/s
May 1992 to Nov. 1992	0.115 ± 0.024
Oct. 1992 to May 1993	0.166 ± 0.020
May 1993 to Nov. 1994	0.174 ± 0.014

Table 3. Estimates of $\partial K/\partial h$

Period	$\partial K/\partial h$, 10^{-8} m/s
May 1992 to May 1993	1.5 ± 2.5
May 1993 to Nov. 1994	2.0 ± 2.0
May 1992 to Nov. 1994	2.0 ± 2.0

and quite close to the level calculated from the Garrett and Munk model spectrum for the internal wave field, following *Gregg* [1989] and *Gregg and Kunze* [1991]. The only anomaly of elevated shear in the record occurred in October 1992, just at the boundary of the two periods for which we have measurements of K, and it is impossible to assign this elevated shear to one period or the other. Thus the internal wave shear level at the mooring does not offer an explanation for the low diffusivity for summer 1992. Although the tracer moved west during the experiment, away from the current meters, a spatial pattern in K in the region of the tracer patch is not suggested by Figure 21. Hence the variation in K between the two phases of the experiment remains unexplained.

The least squares analysis of the tracer dispersion yields estimates of $\partial K/\partial h$ and of $\overline{w}_d$, although with far less accuracy than for K. One can distinguish between the effects of $\partial K/\partial h$ and w because the former distorts the tracer patch through the term on the right-hand side of (7), while a depth-independent velocity does not. A constant positive $\partial K/\partial h$ would cause the peak of a Gaussian distribution to migrate downward with velocity -2 $\partial K/\partial h$, while the center of mass of the distribution would migrate upward with velocity $\partial K/\partial h$, resulting in a distorted profile. Thus the symmetry of the mean tracer profiles, seen even after 30 months, allows useful estimates to be made for $\partial K/\partial h$, although the uncertainties are large (Table 3). The best estimate is 2 ± 2 x 10^{-8} m/s for the full 30-month period. The downward motion of the peak of the tracer distribution appears to be due mostly to a diapycnal velocity $\overline{w}_d$ of -9 ± 3 x 10^{-8} m/s, i.e., approximately -3 m/yr. This velocity will be discussed in the next section.

Thus the data seem to indicate that $\partial K/\partial h$ is not less than zero and is most likely positive. It is reasonable for K to increase upward, since the density ratio decreases upward (Figure 3) and therefore the contribution to K from salt fingering might increase upward. Indeed, an extensive survey surrounding the tracer release site with a free-falling microstructure profiler in April 1992 indicated that the diapycnal diffusion in the region of the patch was influenced by salt finger mixing [*St. Laurent and Schmitt*, 1998]. Applying a model for the effect of salt fingers to the measurements of dissipation of kinetic energy and temperature variance, these authors estimate that the eddy diffusivity for salt K_S at 300 dbar was approximately 0.13 cm^2/s, increasing upward with $\partial K_S/\partial z \approx 5$ x 10^{-8} m/s between 400 and 200 dbar, and 1.6 times as large as the eddy diffusivity for heat K_θ in this depth range. The eddy diffusivity of the tracer K should be close to K_S because the molecular diffusivity of the tracer is similar to that of salt. to that of salt. Thus both the magnitude and the vertical gradient of K are consistent with estimates of K_S by *St. Laurent and Schmitt* [1998].

In summary, the mean value for K in the region of the subtropical pycnocline sampled by the tracer was 0.17 cm^2/s, averaged over 2 years and over more than 10^5 km^2. The data from the first phase of the experiment indicate that temporal or spatial fluctuations at least as large as 0.05 cm^2/s can occur for areas of 10^4 km^2 and periods of 6 months. The vertical gradient of the diapycnal diffusivity may have been greater than zero but was probably not larger than 4 x 10^{-8} m/s.

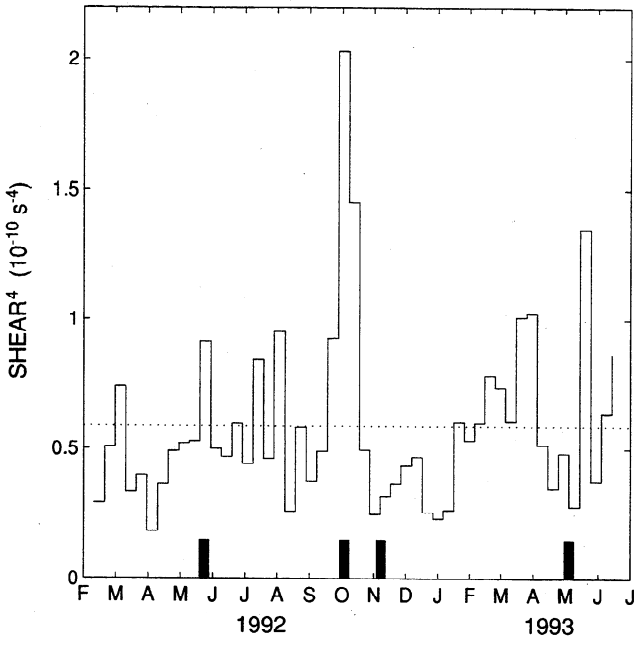

Figure 27. Ten-day means of the fourth power of 10-m shear from the current meters at 300- and 310 m depth. The times of the surveys are indicated by the heavy lines. The dotted line indicates the level expected for the Garrett and Munk internal wave model spectrum.

5. Diapycnal Velocity

The depth of the target density surface in the area of the patch increased as the patch moved west, but this along-isopycnal subduction of 50 or 60 m during the 30

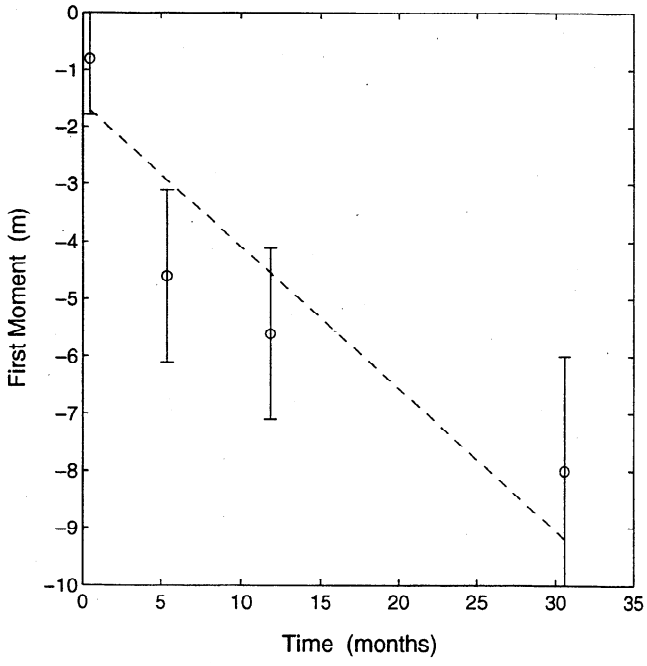

Figure 28. First moment of the Gaussian fits to the mean tracer profiles. The data from October and November 1992 have been combined into one point at approximately 5 months. The dashed curve is a least squares fit to a straight line.

months of the experiment served only to increase the distance from the target surface to the bottom of the winter mixed layer. Of greater interest is the downward motion of the center of mass of the tracer relative to the target isopycnal surface (Figure 28). Estimates of the first moment of the vertical tracer distribution, and hence of the diapycnal velocity $\overline{w}_d$, suffer from a source of error which affects the estimates of K very little, namely the calibration of the CTD sensors. An offset of 0.002 deg in temperature corresponds to an error of 0.3 m in the first moment of the tracer distribution; 0.002 parts per thousand in salinity correspond to 0.9 m. Absolute errors this large are possible in spite of efforts at careful calibration with a salinometer on board each ship and timely laboratory temperature calibrations. Nevertheless, the data clearly indicate a $\overline{w}_d$ of -2 to -4 m/yr.

Several processes have been considered that would lead to a sinking of this magnitude. One is transport of SF_6 on sinking particles due to adsorption and desorption. Experience with sampling gear has shown that SF_6 dissolved in water will adsorb onto surfaces, as mentioned in section 3.4. Crude extrapolation of the adsorption coefficient from smooth plastic surfaces to sinking particulates at 300-m depth in the ocean suggests that transport by particles of three meters per year is not out of the question. Adsorption coefficients for SF_6 onto relevant types of particles have yet to be measured, and the particle distributions and fall rates in oligotrophic waters are under active study. Attributing the downward transport of SF_6 to particle transport with any confidence must await further work.

It is also possible that the water itself is moving downward through isopycnal surfaces. One process that is continually tending to make water denser during mixing events is cabbeling, associated with the dependence of α and β, defined in section 3.1, on pressure, temperature, and salinity [e.g., *McDougall*, 1987]. However, rough calculations of the contribution of cabbeling to $\overline{w}_d$ from either isopycnal or diapycnal mixing give values on the order of -0.1 m/yr.

Another process that will contribute to $\overline{w}_d$ is convergence of heat or salt due to diapycnal mixing. Setting aside contributions from cabbeling and other nonlinearities in the equation of state, the time derivative of the density following the fluid is

$$\frac{d\sigma}{dt} = -\rho\alpha\left[K_\theta\frac{\partial^2\theta}{\partial h^2}+\frac{\partial K_\theta}{\partial h}\frac{\partial\theta}{\partial h}\right] +\rho\beta\left[K_S\frac{\partial^2 S}{\partial h^2}+\frac{\partial K_S}{\partial h}\frac{\partial S}{\partial h}\right] \quad (8)$$

where the reference pressure for both σ and θ should be the local pressure. *St. Laurent and Schmitt* [1998] have estimated a diapycnal velocity of -1.7 ± 1.2 m/yr from this equation, a little shy of the observed $\overline{w}_d$. As mentioned earlier their estimates of K_S and its vertical gradient, on the basis of microstructure data and a model of salt finger fluxes, are consistent with our estimates of K.

In summary, it is not clear what processes caused the tracer to sink relative to the density surfaces. Particle transport is certainly one possibility that bears study but so are various mixing processes. A diapycnal sinking of the water in the pycnocline may contradict conventional images of the thermohaline circulation, but even in the absence of particle transport such sinking may be entirely consistent with the subtle distribution of mixing of heat and salt in the ocean.

6. Lateral Dispersion

6.1. Dispersion of the Initial Streaks

The rms lateral width of the streaks left in the wake of the injection sled σ_{1i} is estimated at tens of meters, based on data gathered by the authors in past field experiments, and on lab studies by *Lin and Pao* [1979]. This width is much smaller than the distance between streaks of approximately 5 km, so the tracer patch began as a set of widely separated streaks. These streaks seemed to have been broadened and juxtaposed to make a nearly continuous patch by the time of the first survey, roughly 14 days after injection (Figure 7). We interpret the features seen within this patch with the 18-chamber sampler as streaks that had been stretched, reoriented, and distorted at scales greater than a few kilometers and that had been broadened in the cross-streak direction at smaller scales.

The order of magnitude of both the rate of strain γ_1 tending to stretch the streaks and an effective cross-

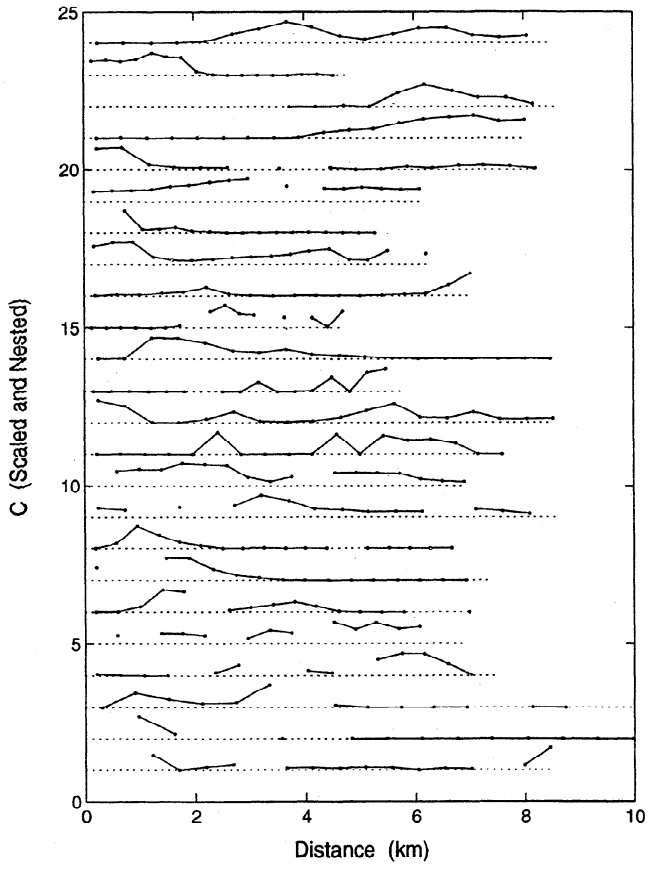

Figure 29. Tracer transects from the multichamber samplers from May 1992. The transects are ordered sequentially in time, with the latest at the top. Concentrations in each transect have been scaled by dividing by the maximum concentration for that transect. Gaps occur where samples were lost.

streak diffusivity K_1 tending to broaden them can be estimated from the area actually tainted by the tracer at the time of the first survey, and the characteristic width of the streaks at that time. The records from the 18-chamber sampler (Figure 29) were examined for segments that could be interpreted as complete crossings of individual streaks. More than 40 such segments have been identified, although not all of them are completely delimited and resolved because of missing samples. The mean width of these segments is around 2 km, and, allowing for crossing at various angles and for the finite resolution of the samplers, we estimate an rms streak width σ_1 of 0.3 ± 0.1 km. The lower bound here allows for smoothly merged streaks being counted as a single streak; the upper bound allows for a tendency to count a "noisy" streak as multiple streaks. A trend toward broader features with time is also noticeable in Figure 29.

If stretching of the streaks were ignored altogether, the cross-streak diffusivity would be estimated as $(\sigma_1^2 - \sigma_{1i}^2)/(2\Delta t)$, or approximately 0.04 m^2/s for $\Delta t = 14$ days. However, broadening of the streaks to an rms width of 0.3 km cannot by itself fully account for the area apparently tainted by tracer. Either we have greatly underestimated the streak width, which would imply a much larger diffusivity than 0.04 m^2/s or there had been some stretching of the streaks. We favor the latter possibility, although, without a better map of the tracer patch, this must be taken as a matter of intuition about the processes of dispersion.

Let us then estimate the overall length L of the streaks at 14 days, assuming an rms streak width of 0.3 km. First, we estimate the minimum area A_t that was tainted by 95% of the tracer. We assume that virtually all of the tracer was within the area sampled although, as noted in section 3.3, the data suggest that some of the tracer may have escaped the survey. We also assume that the concentration distributions along the tow tracks were typical of the patch. Of all the tracer found along the sampling tracks, 95% of it was found along the most tracer-rich 60 km. We estimate A_t from the product of this 60 km and the spacing between the tracks, which was around 5 km, so that $A_t = 300 \pm 100$ km^2. For a Gaussian streak, 95% of the tracer in the cross-streak distribution would be contained within $\pm 2\,\sigma_1$ of the streak center, so L is estimated as $A_t/(4\sigma_1) = 250$ km (160 to 500 km), compared with $L_i = 100$ km initially.

The streak growth is presumed to have been due to strain along each streak element, although shear can also play a role. This strain would not be constant with time, nor uniform along the streak, but it would lead to a growth of the streak length that is exponential in character, with a mean growth rate given by some properly weighted strain rate [*Garrett*, 1983]. Let us simply estimate an empirical streak growth rate of $\gamma_1 = (\Delta t)^{-1} \ln(L/L_i) = (8 \pm 4) \times 10^{-7}$ s^{-1} for $\Delta t = 14$ days, $L_i = 100$ km, $L = 250$ km. The zonal straining of the overall patch by a factor of 2 mentioned earlier could account for the lower bound here, but contributions to stretching by motions within the patch are also suggested by the data. We shall see clearer evidence of efficient dispersion at these scales in the fall 1992 data.

A lateral diffusivity at the scale of the streak width can now be crudely estimated with the aid of a simple model of a tracer streak being stretched at a constant rate γ_1 in the along-streak direction. The strain field will tend to compress the tracer in the cross-streak direction, while smaller-scale processes, represented here by a Fickian diffusivity K_1, will oppose this compression [*Townsend*, 1951]. The equation for the column integral I is

$$\frac{\partial I}{\partial t} + \gamma_1 x \frac{\partial I}{\partial x} - \gamma_1 y \frac{\partial I}{\partial y} = K_1 \left[\frac{\partial^2 I}{\partial x^2} + \frac{\partial^2 I}{\partial y^2} \right] \quad (9)$$

where t, x, and y denote time, the along-streak coordinate, and the cross-streak coordinate.

Equations for the zeroth and second moments of the cross-streak distribution may be found by multiplying

this equation by y^0 and by y^2 and integrating over all y. The following equation for σ_1^2, the ratio of the second to the zeroth moment, can then be found:

$$d\sigma_1^2/dt = 2(K_1 - \gamma_1\sigma_1^2) \tag{10}$$

with the solution:

$$\sigma_1^2 = (\sigma_{1i}^2 - K_1/\gamma_1)e^{-2\gamma_1 t} + K_1/\gamma_1 \tag{11}$$

This model accounts for time dependence in the streak width but not in the local strain rate. At $t = 14$ days the transient term in (11) is already small, so we have $K_1 \approx \sigma_1^2\gamma_1$. The resulting estimate for K_1 is (0.07 $\pm$ 0.04) m^2/s, for $\sigma_1 = 0.3 \pm 0.1$ km and $\gamma_1 = (8 \pm 4)$ x 10^{-7} s^{-1}. Note that this estimate is similar to the estimate obtained earlier, with strain ignored, so that the order of magnitude of K_1 does not seem particularly sensitive to the refinement of the model for the time scales examined here.

These estimates of K_1 are somewhat larger than can be attributed to shear dispersion due to internal waves. *Young et al.* [1982], analyzing the dispersion due to various frequencies of shear, showed that to a good approximation the lateral diffusivity due to internal waves interacting with K is

$$K_{iw} \approx \frac{K}{2}\int_f^N \int_0^{m_*} \frac{S(\omega,m)}{\omega^2}\, d\omega\, dm \tag{12}$$

where K_{iw} is the diffusivity in one of the lateral directions due to the internal wave shear, f is the inertial frequency, N is the buoyancy frequency, $m_* = \sqrt{\omega/K}$ is a cutoff vertical wavenumber associated with the "Taylor limit" of shear dispersion, $S(\omega, m)$ is the shear spectrum of the internal wave field, and K is the diapycnal diffusivity.

The shear variance at the site can be estimated from the record of the velocities at 300- and 310-m depth at the current meter mooring, whose location is shown in Figure 11. The frequency spectrum of the difference between these velocities is dominated by a peak at the inertial period, although the ω^{-2} dependence expected of the internal wave field is weakened by Doppler shifting to high frequencies. This shifting should not affect the total variance, which for the period of February to October 1992 is

$$< (\Delta u)^2 + (\Delta v)^2 > = 6.0\,\mathrm{cm}^2/\mathrm{s}^2 \tag{13}$$

The value for May 1992, the time of the injection and first survey, was the same, but note that the patch was 60 km from the current meter at this time (Figure 11). Such a measurement is sensitive to calibration errors of the two current meters, but confidence in the measurement is high because strong tidal peaks which appear in the individual velocity spectra do not appear in the difference spectra.

The mean square velocity difference at 10-m separation expected from the Garrett and Munk internal wave spectrum [*Gregg*, 1989; *Gregg and Kunze*, 1991], is 5.3 cm^2/s^2 at the values of N and f for the site, quite close to the observed value. This mean square difference is insensitive to the shear spectrum at wavenumbers beyond 0.1 cpm, where the wavenumber dependence of the spectrum changes from m^0 to m^{-1} [*Gargett et al.*, 1981]. If we assume this shape for the spectrum, as did *Young et al.* [1982], and scale it with the observed mean square velocity difference, then (12) gives $K_{iw} = 2400$ K. The diapycnal diffusivity K during this period was no greater than 1.0 x 10^{-5} m^2/s, estimated from the growth of the diapycnal distribution of the tracer from a delta function to the Gaussian shown in Figure 10. Hence we have

$$K_{iw} < 0.024\,\mathrm{m}^2/\mathrm{s} \tag{14}$$

The upper limit here is a bit below the range of reasonable values estimated for K_1 above. It is very dependent on the separation of the spectrum into a function of ω times a function of m. Nearly all the contribution to the integral comes from $\omega < 2f$, and 60% of it comes from $m > 0.1$ m^{-1}. If the high wavenumber region does not have the same inertial peak as the rest of the spectrum, the estimate in (14) would be considerably smaller.

It seems most likely that processes at subinertial frequencies contributed to the observed dispersion, especially in light of the large diffusivities inferred at larger scales discussed in the next section. The advantage of low frequency in shear dispersion is clear from the ω^{-2} dependence in the integrand of (12). As pointed out by *Young et al.* [1982], shears associated with finestructure in the density field could be effective at lateral mixing. *Polzin et al.* [1995b] proposed that vortices driven by anomalies in the stratification would contribute strongly to shear dispersion. The shears involved would be feeble compared with internal wave shears, but their persistence in a reference frame moving with the tracer patch would more than compensate.

In summary, it appears that the lateral dispersion of tracer at scales of 0.1 to 1 km occurs at a rate which is too large to be accounted for by shear dispersion by the internal waves but could be due to shear at subinertial frequencies. This dispersion acted to broaden streaks to create the features with rms width of ~0.3 km seen by the multichamber sampler, while the overall length of the streaks was growing by a factor of ~2.5 by a straining process acting at larger scales.

6.2. Lateral Dispersion at Scales of 3 km

It is apparent from Figure 11 that the tracer patch had again become severely streaky by the time of the fall 1992 survey, 5 and 6 months after the injection, but now at scales of hundreds of kilometers. The mesoscale eddy field had apparently teased the tracer patch into long streaks as envisioned by *Garrett* [1983], and as modeled

by *Haidvogel and Keffer* [1984], *Holloway and Kristmannsson* [1984], and *Sundermeyer and Price* [this issue].

The length of the streaks found at this time, measured along their sinuous tracks, was approximately 600 ± 200 km, the uncertainty arising from motions of the patch during sampling. The amount of tracer found was about a third of the amount injected, so the overall streak length must have been around 1800 km (1000 to 3000 km) if the unsampled streaks were similar to those sampled.

The patch observed in May 1992, 14 days after injection, may be viewed as a nascent streak already being stretched by the mesoscale eddy field. The length of this patch was 50 km, so the effective streak growth rate for the period from May to November was $\gamma_{10} = \ln(1800/50)/5.5$ months $= (3 \pm 0.5) \times 10^{-7}$ s^{-1}, as reported by *Ledwell et al.* [1993]. We distinguish between γ_{10} in this section and γ_1 in the previous section because the analysis now reflects the actions of 100-km scale eddies rather than the 10-km scale of motions acting on the early tracer patch. The assumption of an exponential growth at the mesoscale is on firmer ground here than for the 10-km scale of the previous section. *Garrett* [1983] argued that such a growth regime would prevail, with the growth rate expected to scale with the rms strain rate of the velocity field. The numerical simulations of *Haidvogel and Keffer* [1984] and *Sundermeyer and Price* [this issue] have confirmed this. Sundermeyer and Price have shown with an ensemble of realizations from a kinematically realistic numerical model that the growth rate calculated from the streak length 3 months after release is between a third and a sixth of the rms strain rate calculated from the strain tensor for the velocity field. They found the streak growth rate to be more nearly equal to the rms value of the strain in the along-streak direction within the streak, as might be expected.

Although the tracer patch was severely streaky in fall 1992, the width of the streaks was large enough to imply remarkably efficient cross-streak dispersion. An accurate estimate of the rms streak width is not possible, since only a fraction of the tracer was found, and even then it is only for that part of the patch for which the boundaries of the streaks can be identified. The two ends of the streak sampled in October 1992 were rather complicated, and the cross-streak resolution was poor for the November survey. Assuming some folding and branching at the ends of the streak observed in October, we estimate that the rms streak width σ_{10} was 3 km (2 to 5 km). Lateral dispersion in the cross streak direction is required to maintain this rms streak width in the presence of along-streak strain, as discussed above for smaller scales. Equation (11) should still be useful, with γ_1 replaced by γ_{10}, σ_1 replaced by σ_{10}, and K_1 replaced by K_{10}, an effective diffusivity acting at 10-km scale. The quantity $e^{-2\gamma_{10}t}$ is very small at $t = 6$ months, so if γ_{10} had been uniform in space and time, the rms streak width would be steady at this point, and we would simply estimate K_{10} as

$$K_{10} \sim \sigma_{10}^2 \gamma_{10} \tag{15}$$

which gives a value of 3 m^2/s (1 to 10), i.e., more than an order of magnitude larger than K_1 estimated in the previous section for features with rms widths of 0.3 km.

A large uncertainty is assigned to K_{10}, mostly because the streak growth rate is by no means uniform in space and time. The strain rate following a segment of the streak will vary on the same time scale, $1/\gamma_{10}$, over which a steady state would be reached, so the steady state approximation is imperfect and may lead to a bias in the estimate of K_{10}, although it is not clear which direction the bias would be. Furthermore, there may be strong variations in the along-streak strain rate as one crosses the streaks, as found by *Sundermeyer and Price* [this issue] in their numerical simulations. It seems likely that the streak growth would reflect the largest strains along the streak, while the cross-streak diffusivity setting the streak width needs to counteract only some cross-streak average of the strain. If this is true, then (15) overestimates K_{10}. In fact, *Sundermeyer and Price* [this issue] have run an ensemble of realizations with velocity and length scales very similar to those of the NATRE area, as determined from the statistics of float trajectories, and with K_{10} set at 10 m^2/s and model resolution of 1.2 km. They find that with γ_{10} estimated from the streak length in the model, and with σ_{10} estimated from samples across a streak of tracer dispersing in the model, (15) overestimates the K_{10} by a factor of 2. Taking these model results into account, we lower our estimate of K_{10} to 2 m^2/s (0.6 to 6).

The processes responsible for the cross-streak diffusivity have not been identified, although candidates have been proposed. A possibility mentioned in the previous section is shear dispersion at subinertial frequencies, as suggested by *Young et al.* [1982]. *Polzin et al.* [1995b], have estimated that vortical modes perceptible in the fine structure observed at the site of the experiment could give $K_{10} \approx 2$ m^2/s.

Thermohaline intrusions have also been suggested by a reviewer as a possible mechanism of dispersion at these scales (see *Ruddick and Hebert* [1988] for an overview). *Hebert et al.* [1990] concluded that the slow decay of the salinity anomaly of a Meddy observed closely for several years was due to isopycnal mixing driven by thermohaline intrusions. The effective diffusivity inferred was 1 to 2 m^2/s, at 20-km scale. This is near the value we infer at very similar scale for the tracer streaks, which are in the same part of the ocean as Meddies, but well above them. However, the salinity gradients on isopycnal surfaces that drive intrusions are at least an order of magnitude smaller at the level of the tracer patch than across Meddies. Hence we are skeptical that thermohaline intrusions are responsible for the dispersion observed but cannot rule them out.

The current meter data from the central mooring of the Subduction Experiment have been examined for estimates of subinertial shear. Velocity differences at 10-m separation are too small, relative to calibration uncertainties, to make estimates at subinertial frequencies. Data from current meters with vertical separations of 100 and 450 m indicate that at these separations there does not appear to be enough shear, with enough persistence, to explain the observed cross-streak dispersion. This conclusion does not rule out low-frequency shear as a mechanism, however. For example, the shears proposed by *Polzin et al.* [1995b] would be of too small vertical scale to be detected at 100-m separation and too short lateral wavelength to persist at a fixed point for very long. The efficient cross-streak dispersion at 10-km scale remains an interesting result for further investigation.

6.3. The 1-Year Survey

The patch surveyed in the spring of 1993, 12 months after injection, was nearly continuous, in the sense that tracer was observed with spot casts almost everywhere within the patch. This continuity was in striking contrast with the fall 1992 survey discussed above and confirms the scaling model of *Garrett* [1983] and the numerical model of *Haidvogel and Keffer* [1984] for how such a patch of tracer would homogenize in a field of mesoscale eddies. In these models the overall streak length grows exponentially with time until the streaks begin to overlap with one another, after which time the patch quickly fills in. The time for this to occur estimated by *Garrett* [1983] was of the order of 1 year for the ocean pycnocline. The numerical models of *Haidvogel and Keffer* [1984] and *Sundermeyer and Price* [this issue] agree with Garrett's scale analysis on these points.

Although the spring 1993 patch was continuous, there did remain a rich spectrum of spatial variability. The smallest scales were sampled by the 50-chamber sampler on two 60- to 70-km transects with resolutions of 0.16 to 1.3 km (Figure 30a and 30b). Small fluctuations in concentration at scales smaller than 3 km are reminiscent of the features seen 2 weeks after the injection. Larger fluctuations at scales of 10 km are reminiscent of the streaks found in fall 1992. The edges of these features are sharp in several cases, indicating an edge scale of 1 km, which was also found in the fall 1992 survey. The largest fluctuations in the records have a wavelength approximately equal to the length of the transects and seem composed of patches of the 10-km features.

There are only two independent samples from the high resolution tracks at 65 kilometer wavelength, but the rosette stations (Figure 18) give more information at this and greater length scales. In particular, a 600-km transect with stations every 13 km was obtained at 25.5° N (Figure 31). Concentration peaks and clusters of peaks at a wavelength of around 100 km are apparent in this transect. Fluctuations at the smallest resolvable

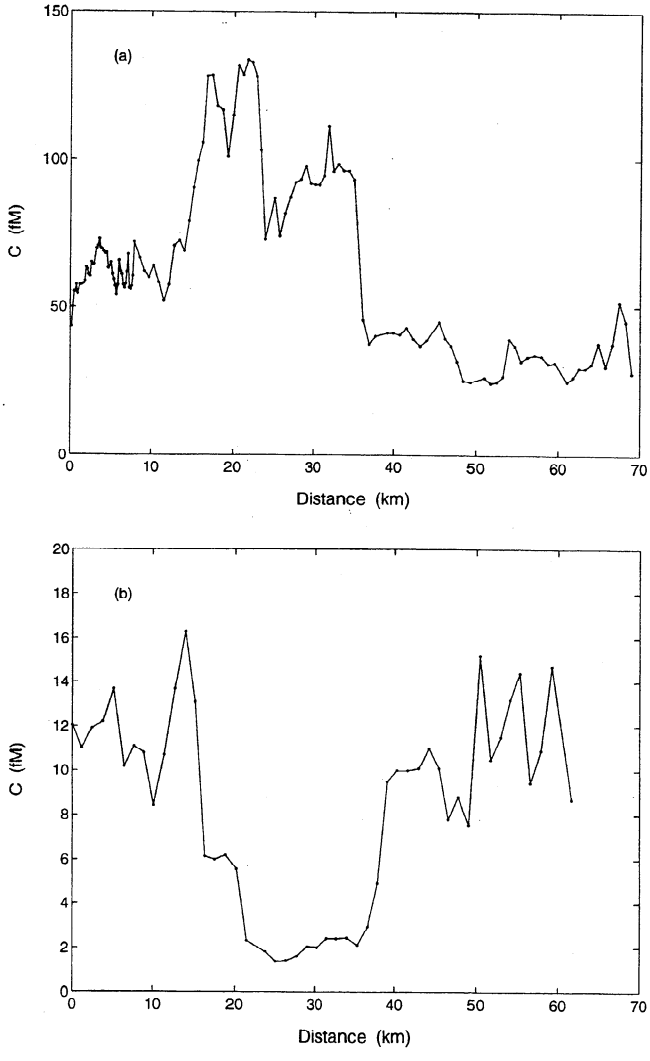

Figure 30. Transect from the multichamber sampler during the May 1993 survey. (a) concantenation of 3 consecutive tracks; (b) a fourth single track. See Figure 18 for track locations.

wavelength of 26 km, seen especially between 31° W and 32° W in Figure 31, suggest large variance at unresolved scales, consistent with the streaks found in fall 1992 and in the 50-chamber tows at 10-km wavelength.

A means of quantifying the spatial homogeneity of the patch which will be useful for comparison with the 30-month survey is the spatial autocorrelation of the concentration field. This function has been estimated from all the available pairs of rosette stations in the survey, sorted into bins of distance of separation $r_k \pm \Delta r/2$, and written as follows:

$$f(r_k) = \frac{\sum_{m=1}^{N}[(I_m - \overline{I}^k)\sum_{n=1}^{N_m^k}(I_n - \overline{I}^k)]}{\sum_{m=1}^{N} N_m^k (I_m - \overline{I}^k)^2} \qquad (16)$$

where $\sum_m^N$ is a sum over all stations; $\sum_n^{N_m^k}$ is a sum over those stations whose distance from station m is in

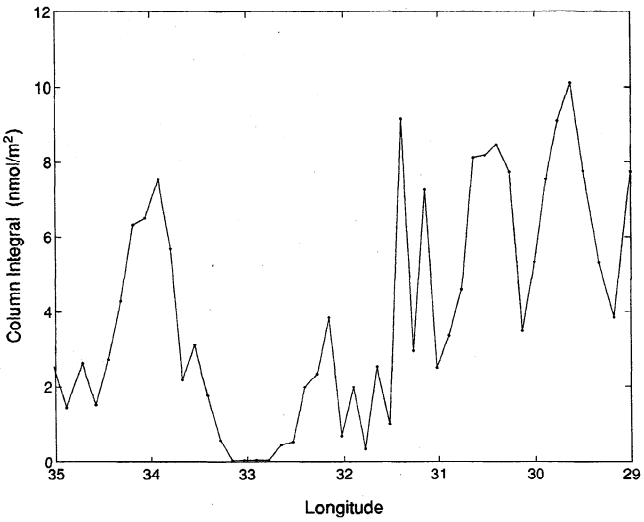

Figure 31. Transect of concentration at the target density surface along 25.5°N from the spring 1993 survey.

the k'th bin, regardless of absolute positions and relative directions. I_m is the vertically integrated tracer concentration, or column integral at station m. $\bar{I}^k$ is the average of the column integrals, with each column integral I_m weighted by the number of times N_m^k that I_m is a member of a pair:

$$\bar{I}^k = \frac{\sum_{m=1}^{N} N_m^k I_m}{\sum_{m=1}^{N} N_m^k} \tag{17}$$

No corrections for advection during the survey have been made, and this may decrease the estimated autocorrelation, especially at the smaller scales. The zero crossing of $f(r_k)$ is approximately 160 km (Figure 32); the integral of $f(r_k)$ from $r_k = 0$ to 160 km is approximately 40 km. These will be used as length scales characterizing the homogeneity of the patch.

6.4. The 30-Month Survey

The patch had become more homogeneous at 30 months, in the sense that the length scales of the lateral autocorrelation had increased (Figure 33). Smoothing the autocorrelation function, we estimate the zero crossing to be at approximately 400 km, more than twice the 12-month value. The integral from $r_k = 0$ to this zero crossing had increased from 40 to 140 km.

Although only about half of the patch was sampled at 30 months, the observations shown in Figure 23 suggest that the remainder of the tracer lay to the east. To speculate how the patch might lay and to obtain rough estimates of the moments of the patch, the data were fit by the method of least squares to a two-dimensional Gaussian function of the form:

$$I(x,y) = \frac{N}{2\pi}\sqrt{\frac{1}{a^2b^2} - c_1^2} \cdot \exp\left\{-\frac{(x-x_0)^2}{2a^2} - 2c_1(x-x_0)(y-y_0) - \frac{(y-y_0)^2}{2b^2}\right\} \tag{18}$$

to determine the parameters a, b, c_1, x_0, and y_0. The total amount of tracer N was kept fixed at 951 moles. The fit returned an estimate for c_1 that is virtually zero, in which case the axes of the ellipses of constant concentration are aligned with the zonal and meridional axes, and the second moments along the axes σ_x^2 and σ_y^2 are given simply by a^2 and b^2, respectively. The results for the various moments are listed in Table 1.

The best fit 2-D Gaussian is mapped in Figure 34, and the data are compared with this function in Figure 35. The mean square deviation of the observations from the Gaussian function is three times smaller than the variance of the concentrations. It appears from Figure 34 and from other mapping approaches that a little over half of the tracer was west of 37.5°W. Uncertainty estimates for the moments from this survey reported in Table 1 are based on scenarios of how the unsam-

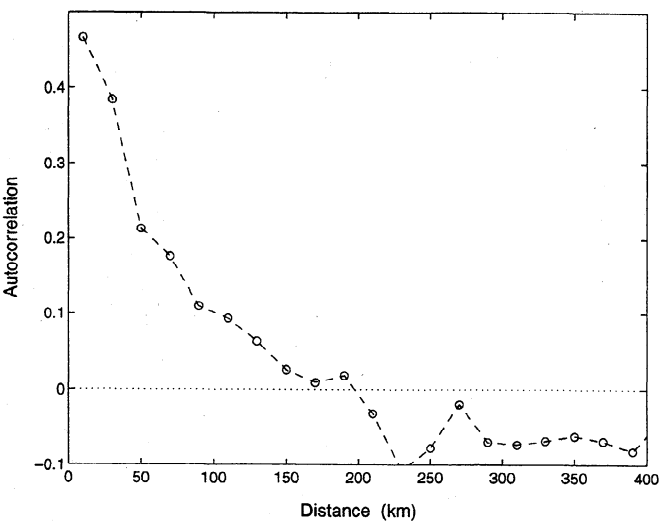

Figure 32. Spatial autocorrelation of the column integral of tracer for spring 1993.

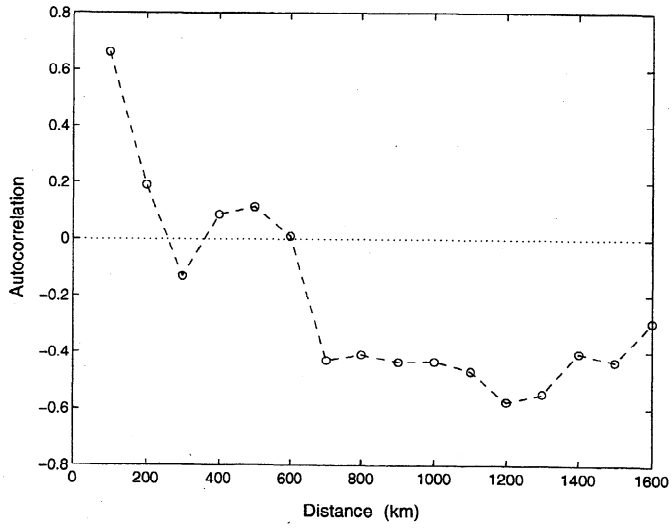

Figure 33. Spatial autocorrelation of the column integral of tracer for November 1994.

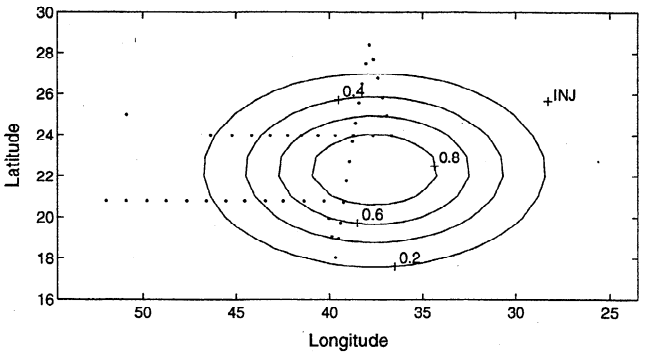

Figure 34. Best fit two-dimensional Gaussian to the column integral for November 1994. Stations are indicated by dots. The contours are in nmol/m^2, and the injection site is indicated. The center of the Gaussian fit lies to the east of the stations.

pled half of the tracer might have been distributed, and therefore are highly subjective.

6.5. Lateral Movement of the Patch

Velocities of the patch between surveys can be estimated from the positions of the center of mass (Table 1). For the first 12 months the drift was approximately west at 1.3 ± 0.4 cm/s. Between 12 and 30 months the drift was 1.3 ± 0.8 cm/s, approximately west-southwest. These drift velocities are in agreement with estimates from the floats by *Sundermeyer and Price* [this issue], and both are consistent with climatological data [e.g., *Thiele et al.*, 1986] and individual hydrographic surveys at various times [e.g., *Armi and Stommel*, 1983; *Bauer and Siedler*, 1988], which suggest a mean flow to the southwest at approximately 1 cm/s.

6.6. Estimates of Lateral Diffusivities at the Mesoscale

Between 12 and 30 months the patch was perhaps large enough compared with the mesoscale eddies to parameterize the zonal and meridional dispersion with Fickian coefficients K_x and K_y. They are estimated as

$$K_x = \Delta\sigma_x^2/(2\Delta t) \quad (19)$$

$$K_y = \Delta\sigma_y^2/(2\Delta t) \quad (20)$$

where the Δ values refer to changes over the 18-month period. The results for σ_x and σ_y for 12 months and 30 months, listed in Table 1, give K_x = 2300 m^2/s (1000 to 4000), and K_y = 650 m^2/s (200 to 1200) from these formulas. These estimates agree with those of *Sundermeyer and Price* [this issue] from the float data, who find values of 1500 ± 700 m^2/s for K_x and 700 ± 400 m^2/s for K_y. The float data indicate that the anisotropy is associated with a difference in the Lagrangian eddy length scales, rather than in the velocity scales in the two directions [*Sundermeyer and Price*, this issue]. Our results are quite uncertain, based as they are on an incomplete survey at 30 months, and should be viewed merely as a check for consistency with estimates from other techniques.

Enhancement of K_x over K_y is expected for geostrophic turbulence on a β plane [e.g., *Holloway and Kristmannsson* [1984]. However, gyre-scale positive strain could have played some role in the zonal stretching of the patch. An analytical calculation starting with an equation of the same form as (9) can be used to show that the growth of zonal and meridional mean square dispersion between 12 and 30 months could be modeled with an isotropic lateral diffusivity of 1100 m^2/s if there were a steady zonal strain of 8 x 10^{-9} s^{-1}. This strain would correspond to an increase in the westward current of 0.4 cm/s between 30° and 35°W, which is below the threshold of detection from the center of mass of the tracer patch, and probably from the floats and other techniques. Hence gyre-scale strain could account for at least part of the apparent anisotropy of the lateral diffusivity estimated from the tracer dispersion.

6.7. Scale Dependence of the Lateral Diffusivity

If the lateral dispersion could be described by a Fickian diffusivity, then the area of the overall tracer patch would have grown approximately linearly with time. It is well known, however, that lateral dispersion in the ocean is not Fickian, but rather that a lateral diffusivity will depend on the scale of motion it is intended to parameterize. We have seen examples of this here, where the effective diffusivity was of the order of 0.07 m^2/s at scales of 0.1 to 1 km, and then of the order of 2 m^2/s at scales of 1 to 30 km, and then again of

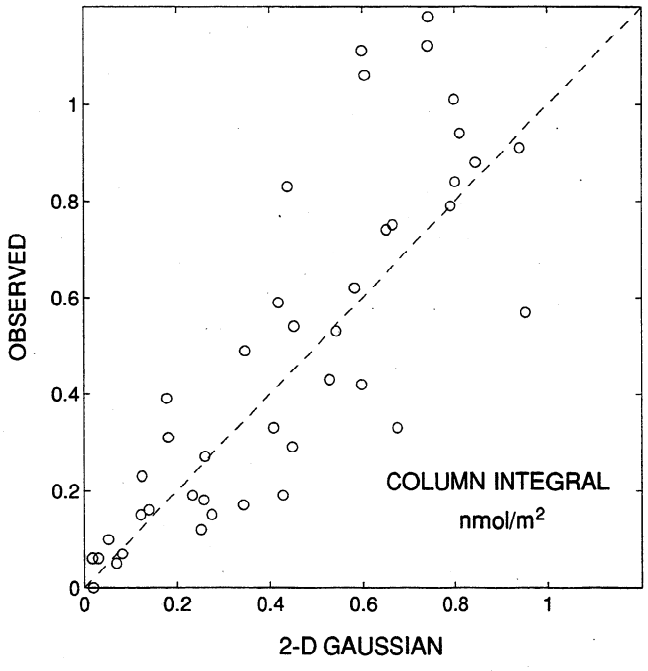

Figure 35. Quality of fit of a two-dimensional Gaussian to the observed column integrals for the November 1994 survey. The dashed line indicates a perfect fit.

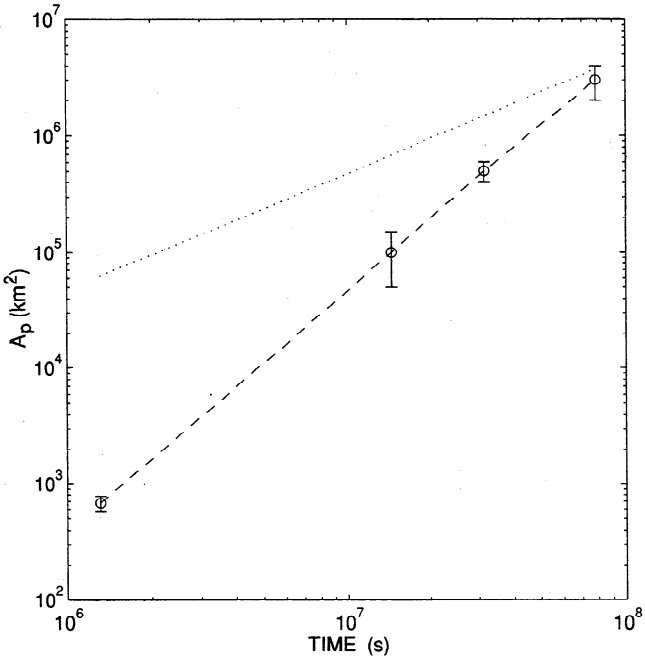

Figure 36. Temporal evolution of the area of the tracer patch. The dotted line represents a linear dependence; the dashed line a quadratic dependence.

the order of 1000 m^2/s at scales of 100 to 1000 km. The first two diffusivities parameterize processes acting within the patch rather than those dispersing the overall patch, but the scale dependence remains evident if the dispersion of the overall patch is examined.

We define an area A_p as the area of the smallest convex figure that can be drawn around the patch, and that encompasses 95% of the tracer. Rough estimates for A_p made for each survey from the maps are listed in Table 1. The data indicate a quadratic dependence of A_p on t (Figure 36), while a Fickian diffusivity D would lead to the linear relation $A_p = 12\pi Dt$ for a Gaussian patch. This idealization is plotted as a dotted line in Figure 36 for $D = 1200$ m^2/s for comparison.

The quadratic dependence is similar to the dependence found by *Okubo* [1971] in his diffusion diagrams for dispersion in oceanic surface waters, where the area of dye patches grew with the 8/3 power of time, approximately. It illustrates once again that a scale-dependent diffusivity is a better model for diffusion of a patch over a variety of scales than a constant diffusivity. The particular quadratic power law for $A_p(t)$ corresponds to an eddy diffusivity which is proportional to the lateral scale, consistent with the diffusion velocity concept attributed to *Joseph and Sendner* [1958]. However, the variety of phenomena underlying Figure 35 discourages too simplistic an interpretation. Mesoscale eddy processes may dominate the middle two points of the plot, but the first point is dependent on the initial condition and on submesoscale processes, while the last point may be influenced by gyre-scale strain, as we have mentioned. We reiterate that a lateral eddy diffusivity in the ocean must be chosen with careful attention to the relevant scale.

6.8. Summary of Lateral Dispersion Results

The tracer experiment yielded the following results for lateral dispersion at 300- to 400-m depth in the southeastern region of the subtropical gyre in the North Atlantic:

1. The initial tracer streaks, less than 100 m wide and 5 km apart, had blended into one nearly continuous patch within 2 weeks of release.
2. This patch grew into a set of sinuous streaks separated by tracer-free waters within a few months.
3. Within a year of release, however, the streaks had grown so much in length as to fill in a broad region, as predicted by *Garrett* [1983] and *Haidvogel and Keffer* [1984].
4. Although the patch was painted in after 12 months, complete homogenization of the tracer within the patch proceeded more slowly, as indicated by the length scales of the autocorrelation function. Even at 30 months, a third of the tracer variance appeared to be at scales of less than 100 km.
5. If an eddy diffusivity is invoked to describe dispersion at scales of 0.1 to 1 km, a value K_1 on the order of 0.07 m^2/s is estimated, larger than expected from the interaction between internal wave shear and diapycnal dispersion.
6. Dispersion at scales of 1 to 30 km is surprisingly efficient. An effective lateral diffusivity K_1 on the order of 2 m^2/s would be required to simulate this dispersion. The processes responsible for dispersion at these scales are not well known, but may be shear dispersion by vortical motions, as proposed by *Polzin et al.* [1995b].
7. Dispersion at scales of 30 to 300 km is dominated by the growth of streaks due to strain in the mesoscale eddy field. The effective streak growth rate γ_{10} was approximately $(3 \pm 0.5) \times 10^{-7}$ s^{-1}. At these scales, use of an eddy diffusivity seems particularly inappropriate, perhaps only because in this case the survey resolves the effects of individual eddies.
8. At scales from 300 to 1000 km, i.e., larger than the scales of the eddy field, perhaps an eddy diffusvity model may again be appropriate. The eddy diffusivity estimated from the tracer dispersion was consistent with the estimates by *Sundermeyer and Price* [this issue] of 1500 ± 700 m^2/s for the zonal diffusivity and 700 ± 400 m^2/s for the meridional diffusivity. This estimate is also consistent with estimates by *Armi and Stommel* [1983], *Joyce et al.* [1998], and *Jenkins* [1987, 1998], for this region of the ocean.

7. Discussion

The diapycnal diffusivity $K = 0.17$ cm^2/s measured in this experiment represents an average over a 2-year period, for a layer about 100 m thick centered at σ_θ

$= 26.75$ kg/m^3 in the region between 20°N and 26°N and between 30°W and 45°W. The diffusivity appears to have been only two thirds as large for an area of 10^4 km^2 near 30° W, 25° N during the first 6 months of the experiment. These differences may reflect the magnitude of variations that exist in the subtropical gyre on such time and space scales.

One immediate source of energy for diapycnal mixing in the region is the internal wave field. The amplitude of the fourth power of the shear was apparently within 10% of that expected from the empirical internal wave spectrum of Garrett and Munk, as would be calculated by *Gregg* [1989] at the current meter mooring positioned near the eastern edge of the patch for the first year. Internal wave data from other sites within the patch are fragmentary but should be examined to characterize the climate of the observed mixing.

The stratification has long been considered to be an important background parameter controlling diffusivity, especially when the immediate energy source is the internal wave field [e.g., *Gargett*, 1984]. However, *Gregg* [1989], *Toole et al.* [1994], *Polzin et al.* [1995a], and *Kunze and Sanford* [1996] have recently provided evidence that the diapycnal diffusivity for density, when it is the result of instability in the background internal wave field, is independent of buoyancy frequency in the stratified open ocean. In the layer occupied by the tracer patch the buoyancy frequency decreased with depth by about 10% per 100 m (Figure 3). The results of the present experiment do not constrain the depth dependence of K well; the best estimate from the tracer data is that K decreases by 0 to 20% per 100 m of depth.

Such a dependence of K on depth is the opposite of what might be expected from the depth dependence of the density gradient, but salt fingering may play a role at this site in addition to internal wave breaking. The density ratio was between 1.9 and 1.7 in the layer occupied by the tracer, decreasing upward (Figure 3), as noted in section 3.1. *St. Laurent and Schmitt* [1998] have attributed a considerable fraction of the dissipation of thermal variance in the layer to salt fingering. The tracer has a molecular diffusivity in seawater of approximately 1×10^{-5} cm^2/s [*King and Saltzman*, 1995], comparable to that of salt, and so should behave in the ocean like salt rather than heat. *St. Laurent and Schmitt* [1998] attribute about half of the dissipation events to salt fingering, and infer that K_S is nearly 1.6 times K_θ, when both shear-driven and finger-driven mixing are accounted for. Hence the possibility that K is larger than K_θ must be considered when applying the results of the present experiment to other areas of the ocean. The influence of salt fingering may help to explain why K might decrease with depth at the present site, since the density ratio increases with depth.

The value of K that we have measured, possibly enhanced by salt fingering, is nevertheless quite small in many contexts. It places strong limitations on heat and salt fluxes in models of the thermocline, for example, and lends credence to ideal fluid models of the thermocline such as those initiated by *Welander* [1959] (see *Huang* [1991] for a review). It also implies a diapycnal flux of nitrate through the upper part of the permanent pycnocline of the order of 0.01 M m^{-2} yr^{-1}, as reported by *Ledwell et al.* [1993]. This is only a small fraction of the flux inferred from in situ oxygen and ^{3}He budgets by *Jenkins* [1988].

A great deal was learned about sampling strategy in this experiment. If one were interested only in diapycnal diffusivity, then, having sampled the initial condition, one is wise to wait until the tracer has been stirred into a continuous patch before a second sampling. It is then relatively easy to obtain enough profiles to establish a stable average for the diapycnal spread, at least for a site as homogenous as the eastern part of a subtropical gyre. A little guidance from neutrally buoyant floats released with the tracer and from historical hydrographic data on the mean flow was sufficient to direct us to the patch.

The processes of lateral mixing are more difficult to measure with a tracer release experiment, although such an experiment yields information that is unattainable by other means. The most surprising of the results on lateral dispersion just summarized in section 6.8, and indeed of the whole experiment, was the efficient cross-streak dispersion inferred from the rms streak width of 3 km found in fall 1992. The effective cross-streak diffusivity of 2 m^2/s acting at this scale implies a process such as shear dispersion by vortical modes [*Polzin et al.* 1995b], and bears further study.

Comparison of the diapycnal diffusivity estimated from the tracer with that estimated from measurements of microstructure and fine structure by *Schmitt et al.* [1994], *Sherman and Davis* [1995], *Duda and Jacobs* [1995], *Ruddick et al.* [1997], and *St. Laurent and Schmitt* [1998], shows that the techniques agree reasonably well. This conclusion lends credence to many estimates made from profiling instruments in the past 2 decades and also to parameterizations of the diffusivity based on the flow of energy to high wavenumbers in the internal wave field *Henyey et al.*, 1986; *Gregg*, 1989; *Polzin et al.*, [1995a].

Important questions remain. How are the diffusivities of heat and salt modulated by the density ratio in the world ocean and what effect does this modulation have on water mass modification and the general circulation? Is K really of order 0.1 cm^2/s throughout the water column over most of the ocean as indicated by the profiler results of *Gregg* [1989], *Polzin et al.* [1995a], *Kunze and Sanford* [1996], and *Polzin et al.* [1997], or does it rise to 1 cm^2/s at mid depths to satisfy the basin-wide balance discussed by *Munk* [1966]? *Polzin et al.* [1997] find evidence for enhanced mixing over rough topography throughout the water column. How important is

this to heat and salinity budgets at middepth? More generally, where does significant diapycnal mixing take place in the ocean, and how?

Appendix

The tracer maps have been made with kriging, following *Journel and Huijbregts* [1978]. The simplest form of kriging, called ordinary kriging, is identical to objective analysis with an unknown but stationary mean, as described by *Bretherton et al.* [1976]. In either case, if one confines the stations to be used for an estimate of the concentration in a grid block to a finite search circle centered on that block, an unknown ensemble mean is reset for each grid block, allowing in effect for the mean to be nonstationary. An elaboration of kriging which allows not only a nonstationary mean, but also a nonstationary gradient in each search circle has been used for the maps here to give concentration estimates which usually fall rapidly to zero in the fringes and to give uncertainty estimates which rise rapidly in the fringes due to the extrapolation involved. This method would be called "unbiased kriging of order three" by *Journel and Huijbregts* [1978]. Their development is sketched here to provide the context of the estimates of the covariance matrices which are used to estimate the uncertainties in the total amount found and in higher lateral moments of the tracer distributions.

It is important in developing a mapping approach using statistical methods to clearly conceive the ensemble over which averages are to be defined. One can imagine an infinite set of tracer release experiments in which the initial distribution of the tracer is the same for each. If the motion field is allowed to differ from one realization to another, then the evolution of the patch will be different for each realization, so that the stations, which are chosen during the sampling with the benefit of incoming information, will vary from one realization to another. This ensemble is not suited for kriging, wherein the stations are imagined to be the same for each realization. However, one can further imagine a subset of realizations for which a reasonable choice of sampling stations would be the choice made for the realization in hand. This implies that the larger-scale aspects of the motion field are similar for each realization but that the smaller-scale aspects are free. It is such a subset, still infinitely large, which is the ensemble imagined here.

The true concentration ζ in the search circle around a grid point (x_i, y_i) is decomposed into a mean part, linear drifts with x and y, and a fluctuating part η:

$$\zeta(x,y) = a_{0i} + a_{1i}(x - x_i) + a_{2i}(y - y_i) + \eta(x,y) \quad \text{(A1)}$$

where x and y are zonal and meridional coordinates, and where a_{0i}, a_{1i} and a_{2i} are constant for a fixed search circle, but which vary with the grid point. Because of this variation, and because ζ cannot depend on the grid point, η must depend on the grid point. This aspect is overlooked by *Journel and Huijbregts* [1978], no doubt because the effects on the covariance functions are indeterminate but small. This seems justified if the search radius is large compared with the length scale of the spatial autocorrelation of η, which proves to be the case here.

The kriging algorithm estimates the spatial mean Z_i of ζ within each grid block, defined as follows:

$$Z_i = \frac{1}{A}\int_{A_i} \zeta(x,y)\,dA \quad \text{(A2)}$$

where A is the area of a block. Z_i is estimated from the observations of the concentrations C_α, which can also be decomposed as in (A1), but with the addition of an error ϵ_α, associated with analytical error and with fluctuations at scales for which there is no information:

$$C_\alpha = a_{0i} + a_{1i}(x_\alpha - x_i) + a_{2i}(y_\alpha - y_i) + \eta(x_\alpha, y_\alpha) + \epsilon_\alpha \quad \text{(A3)}$$

where x_α, y_α are the coordinates of the station.

Kriging returns an unbiased estimate Z_i' of Z_i, which is a linear combination of the C_α:

$$Z_i' = \sum_\alpha \lambda_{i\alpha} C_\alpha \quad \text{(A4)}$$

One can look at this as a sum over all observations, but with $\lambda_{i\alpha} = 0$ for stations outside the search window.

To insure that the ensemble mean of Z_i' is the same as the ensemble mean of Z_i, the following constraints are imposed on the coefficients $\lambda_{i\alpha}$:

$$\sum_\alpha \lambda_{i\alpha} = 1 \quad \text{(A5)}$$

$$\sum_\alpha \lambda_{i\alpha}(x_i - x_\alpha) = 0 \quad \text{(A6)}$$

$$\sum_\alpha \lambda_{i\alpha}(y_i - y_\alpha) = 0 \quad \text{(A7)}$$

The coefficients $\lambda_{i\alpha}$ are found from a linear system derived by minimizing the ensemble mean square difference between Z_i and Z_i', subject to the three constraint equations above, with the method of Lagrange multipliers [see *Journel and Huijbregts*, 1978]. The solution requires estimates of three spatial covariance matrices dependent on the covariance of η, the block-to-block covariance:

$$B_{ij} \equiv \frac{1}{A^2}\int_{A_i}\int_{A_j} \overline{\eta(x,y)\eta(x',y')}\,dA\,dA' \quad \text{(A8)}$$

the block-to-station covariance:

$$X_{i\alpha} \equiv \frac{1}{A}\int_{A_i} \overline{\eta(x,y)\eta(x_\alpha,y_\alpha)}\,dA \quad \text{(A9)}$$

and the station-to-station covariance:

$$P_{\alpha\beta} \equiv \overline{\eta(x_\alpha,y_\alpha)\eta(x_\beta,y_\beta)} + \delta_{\alpha\beta}\,\overline{\epsilon_\alpha^2} \quad \text{(A10)}$$

where the overbar denotes an ensemble average.

Table A1. Kriging Parameters for Various Maps

	May 1992 Smoothed	May 1992 Final	Spring 1993 Smoothed	Spring 1993 Final
R_0	0.7	0.7	0.7	0.92
b, km	200	3	1600	5.4
a	1	1	1	0.5
Search Radius, km	10	10	160	160
Resolution, km	2.5	2.5	27.8	27.8

Estimation of the spatial covariance of η for the ensemble is at the heart of the method, and requires judgement. It is not to be estimated from the autocorrelation defined by (9) and (10) of section 6.3, which is for residuals relative to the overall mean of the data, but from the autocorrelation of residuals relative to a field which has been smoothed on the same scale as the search radius to be used in kriging. Preliminary smoothed maps of the tracer fields have been made with ordinary kriging, i.e., with $a_{1i} = a_{2i} = 0$ in (A1) and (A3), with an autocorrelation function ρ of the form:

$$\rho = R_0 \exp\left\{-\left(\frac{r}{b}\right)^a\right\} \tag{A11}$$

where r is the distance between points, and b is a length scale. R_0 is a number between 0 and 1; the smaller it is, the more smoothing is done, i.e., the less weight is attached to nearby stations. For the smoothed maps, R_0 has been taken to be 0.7, a has been taken as unity, and b has been taken to much larger than the search radius, so that it is the latter that sets the spatial scale of the smoothing. The search radius has been chosen large enough so that at most grid blocks at least half a dozen stations are included; 10 km for May 1992 and 160 km for spring 1993. Pertinent parameters used in creating the various maps are listed in Table A1.

In the case of the smoothed maps, kriging is being used merely to smooth the data and to assign appropriate weights to unevenly spaced data, i.e., to "decluster." Residuals are calculated between the observations and this smoothed map. The rms residual is then also mapped using the same mapping parameters as for the smoothed concentration map to estimate a spatially dependent variance $E^2(x, y)$. The rms residual has been found in the cases here to be roughly proportional to the smoothed concentration, as has been found in other applications and dubbed the "proportional effect" [*Journal and Huijbregts*, 1978]. The autocorrelation functions of the residuals, defined by formulas analogous to (9) and (10) in section 6.3, were estimated, and functions of the form of (A11) were fit to them (Table A1). In this case, R_0, b, and a are estimated from the data. The quantity $1 - R_0$ is the fraction of the variance due to analytical error and sampling error. Finally, the covariance function is estimated as

$$\overline{\eta(x,y)\eta(x',y')} = E(x,y)E(x',y')R_0 \exp\left\{-\left(\frac{r}{b}\right)^a\right\} \tag{A12}$$

Two measures of uncertainty in the mapped variable Z_i' were generated. One is calculated with the covariance matrices defined in (A8) through (A10), using (A12). This error variance is used in the estimates of uncertainties of the moments of the patch, discussed below. The second measure of uncertainty is the error variance calculated with covariance matrices that have not been scaled with a position-dependent variance, i.e., with $E(x, y) = 1$ in (A12). This unscaled error variance is enhanced outside the patch, and suppressed inside the patch, relative to the scaled variance, and is used to decide where on the fringes of the patch to terminate mapping. A value of around 0.5 for this unscaled error has proven to make a reasonable border for the maps in the present experiment. This can be interpreted as the place where the error in Z_i' is of the same order as Z_i' itself.

There are many simpler ways to make satisfactory maps than the present one. The motivation for the development here has been to derive estimates of the uncertainty in the lateral moments of the tracer patches.

A1. Lateral Moments

The maps have been used to estimate the amount of tracer found, the center of mass of the patch, and the and spring 1993, listed in Table 1. The relevant integrals can be defined as follows:

$$M_{pq} = \int x^p y^q \, \zeta(x,y) dx \, dy \tag{A13}$$

The quantities of interest are: $M \equiv M_{00}$, the total amount of tracer within the region; $X_{cm} \equiv M_{10}/M$, the zonal coordinate of the center of mass; $Y_{cm} \equiv M_{01}/M$, the meridional coordinate of the center of mass; $\sigma_x^2 \equiv (M_{20} - M_{10}^2)/M$, the mean square zonal displacement, relative to the center of mass; $\sigma_y^2 \equiv (M_{02} - M_{01}^2)/M$, the mean square meridional displacement, relative to the center of mass; and $\sigma_{xy} \equiv (M_{11} - M_{10}M_{01})/M$, the mean covariance of zonal and meridional displacement, relative to the center of mass.

A discretized approximation of (A13) is:

$$M_{pq} \cong A \sum_i x_i^p \, y_i^q \, Z_i \qquad \text{(A14)}$$

where A and Z_i are defined in (A2), and the sum is over a region which ideally encompasses all of the patch. We estimate this as M'_{pq}, defined as in (A14) with Z'_i replacing Z_i.

In practice, the sums have been computed over regions bounded by the 0.5 contour on the map of the unscaled error variance discussed above. Negative concentrations generated in the fringes by the mapping procedure are set to zero in the few grid blocks where they appear.

The error variance of the moments M'_{pq} is

$$\overline{\left(M_{pq} - M'_{pq}\right)^2} = A^2 \sum_{ij} x_i^p \, y_i^q \, x_j^p \, y_j^q \overline{\left(Z_i - Z'_i\right)\left(Z_j - Z'_j\right)} \qquad \text{(A15)}$$

The constraint equations (A5) through (A7) and the antisymmetry of $(x - x_i)$ and $(y - y_i)$ within a grid block cause the unknown mean and drift terms that enter through (A1)–(A4) to vanish from the expansion of (A15), and the error variance is seen to be a function only of the covariance matrices defined in (A8) through (A10):

$$\overline{(M_{pq} - M'_{pq})^2} = A^2 \sum_{ij} x_i^p \, y_i^q \, x_j^p \, y_j^q \left[B_{ij} - 2 \sum_\alpha \lambda_{i\alpha} X_{j\alpha} + \sum_{\alpha\beta} \lambda_{i\alpha} \lambda_{j\beta} P_{\alpha\beta} \right] \qquad \text{(A16)}$$

The uncertainties listed in Table 1 are calculated from this formula. These uncertainty estimates are not formally justified because conditions for the Gauss-Markov theorem which underlies kriging or objective analysis are sacrificed when nonstationary statistics are admitted. Also, there is subjectivity in constructing the covariance function, and the probability distribution of the errors is certainly not Gaussian. The uncertainties reported are merely a reasonable attempt at estimating something akin to one standard error.

Acknowledgments. The tracer experiment is an outgrowth of suggestions by W.S. Broecker, J. Shepherd and J. Lovelock. We thank J. Price, P. Richardson, and R. Davis for sharing float data, and R. Weller for the use of current meter data. We thank S. Becker, J. Bouthillette, N. Brink, D. Ciochetto, E. Clark, K. Doherty, J. Donoghue, T. Donoghue, T. Duda, K. Fairhurst, C. Fernandez, B. Guest, S. Kery, M. Klas, C. Kinkade, M. Liddicoat, K. Lubcke, C. Marquette, A. Martin, P. Nightingale, N. Oakey, R. Oxburgh, H. Rochat, B. Ruddick, G. Stanbrough, M. Sundermeyer, S. Sutherland, K. Tedesco, J. Valdes, J. White, C. Wooding, RVS in the UK, the crews of *Darwin*, *Hudson*, *Oceanus*, and *Seward Johnson*, and our home laboratories for their help with the experiment. We thank E. Kunze, K. Polzin, R. Schmitt, J. Toole, L. St. Laurent, M. Sundermeyer, and an anonymous reviewer for comments and discussion. The experiment has been supported by the U.S. NSF grants OCE-9020492 and OCE-9415598, and the UK Natural Research Council and is part of the World Ocean Circulation Experiment. This is WHOI contribution 9490.

References

Armi, L., and H. Stommel, Four views of a portion of the North Atlantic Subtropical Gyre, *J. Phys. Oceanogr., 13*, 828-857, 1983.

Bauer, E., and G. Siedler, The relative contributions of advection and isopycnal and diapycnal mixing below the subtropical salinity maximum, *Deep Sea Res., 35*, 811-837, 1988.

Bretherton, F. P., R. E. Davis, and C. B. Fandry, A technique for objective analysis and design of oceanographic experiments applied to MODE-73, *Deep Sea Res., 23*, 559-582, 1976.

Duda, T. F., and D. C. Jacobs, Comparison of shear measurements and mixing predictions with a direct observation of diapycnal mixing in the Atlantic thermocline, *J. Geophys. Res., 100*, 13,481-13,498, 1995.

Ewart, T. E., and W. P. Bendiner, An observation of the horizontal and vertical diffusion of a passive tracer in the deep ocean, *J. Geophys. Res., 86*, 10,974-10,982, 1981.

Gargett, A. E., Vertical eddy diffusivity in the ocean interior, *J. Mar. Res., 42*, 359-393, 1984.

Gargett, A. E., P. J. Hendricks, T. B. Sanford, T. R. Osborn, and A. J. Williams III, A composite spectrum of vertical shear in the upper ocean, *J. Phys. Oceanogr., 11*, 1258-1271, 1981.

Garrett, C., On the initial streakiness of a dispersing tracer in two- and three-dimensional turbulence, *Dyn. Atmos. Oceans, 7*, 265-277, 1983.

Gregg, M. C., Scaling turbulent dissipation in the thermocline, *J. Geophys. Res., 94*, 9689-9698, 1989.

Gregg, M. C., and E. Kunze, Internal wave shear and strain in the Santa Monica Basin, *J. Geophys. Res., 96*, 16,709-16,719, 1991.

Haidvogel, D. B., and T. Keffer, Tracer dispersal by mid-ocean mesoscale eddies, I, Ensemble Statistics, *Dyn. Atmos. Oceans, 8*, 1-40, 1984.

Hebert, D., N. Oakey, and B. Ruddick, Evolution of a Mediterranean salt lens: Scalar properties, *J. Phys. Oceanogr., 20*, 1468-1483, 1990.

Henyey, F. S., J. Wright, and S. M. Flatte, Energy and action flow through the internal wave field: an eikonal approach. *J. Phys. Oceanogr., 91*, 8487-8495, 1986.

Holloway, G., and S. S. Kristmannsson, Stirring and transport of tracer fields by geostrophic turbulence, *J. Fluid Mech., 141*, 27-50, 1984.

Huang, R. X., The three-dimensional structure of wind-driven gyres: Ventilation and subduction, *U.S. Natl. Rep. Int. Union Geod. Geophys., Rev. Geophys., Suppl., 29*, 590-609, 1991.

Jenkins, W. J., ^{3}H and ^{3}He in the beta triangle: Observations of gyre ventilation and oxygen utilization rates. *J. Phys. Oceanogr., 17*, 763-783, 1987.

Jenkins, W. J., Nitrate flux into the euphotic zone near Bermuda, *Nature, 331*, 521-523, 1988.

Jenkins, W. J., Studying thermocline ventilation and circulation using tritium and and helium-3, *J. Geophys. Res., 103*, 15,817-15,831, 1998.

Joseph, J., and H. Sendner, Uber die horizontale Diffusion im Meere, *Dt. Hydrogr. Z., 11*, 49-77, 1958.

Journal, A. G., and C. J. Huijbregts, *Mining Geostatistics*, Academic, San Diego, CA, 1978.

Joyce, T. M., J. R. Luyten, A. Kubryakov, F. B. Bahr, and J. S. Pallant, Meso- to large-scale structure of subducting water in the subtropical gyre of the eastern North Atlantic Ocean, *J. Phys. Oceanogr., 28*, 40-61, 1998.

King, D. B., and E. S. Saltzman, Measurement of the diffusion coefficient of sulfur hexafluoride in water, *J. Geophys. Res., 100*, 7083-7088, 1995.

Ko, M. K., N. D. Sze, W.-C. Wang, G. Shia, A. Goldman, F. Murcray, D. G. Murcray, and C. P. Rinsland, Atmospheric sulfur hexafluoride: Sources, sinks and greenhouse warming, *J. Geophys. Res., 98*, 10,499-10,507, 1993.

Kunze, E., and T. B. Sanford, Abyssal mixing: Where it is not, *J. Phys. Oceanogr., 26*, 2286-2296, 1996.

Law, C. S., A. J. Watson, and M. I. Liddicoat, Automated vacuum analysis of sulfur hexafluoride in seawater: Derivation of the atmospheric trend (1970-1993) and potential as a transient tracer, *Marine Chem., 48*, 57-60, 1994.

Ledwell, J. R., and A. Bratkovich, A tracer study of mixing in the Santa Cruz Basin, *J. Geophys. Res., 100*, 20,681-20,704, 1995.

Ledwell, J. R., and B. M. Hickey, Evidence for enhanced boundary mixing in the Santa Monica Basin, *J. Geophys. Res., 100*, 20,665-20,679, 1995.

Ledwell, J. R., and A. J. Watson, The Santa Monica Basin Tracer Experiment: A study of diapycnal and isopycnal mixing, *J. Geophys. Res., 96*, 8695-8718, 1991.

Ledwell, J. R., A. J. Watson, and W. S. Broecker, A deliberate tracer experiment in Santa Monica basin, *Nature, 323*, 322-324, 1986.

Ledwell, J. R., A. J. Watson, and C. S. Law, Evidence for slow mixing across the pycnocline from an open-ocean tracer-release experiment, *Nature, 364*, 701-703, 1993.

Lester, D., and L. A. Greenberg, The toxicity of sulfur hexafluoride, *Arch. Ind. Hygiene Occup. Med., 2*, 348-349, 1950.

Levitus, S., Climatological Atlas of the World Ocean, *NOAA Prof. Pap., 13*, Superintendent of Documents, U.S. Government Printing Office, Washington, D. C., 1982.

Lin, J.-T., and T.-H. Pao, Wakes in stratified fluids, *Ann. Rev. Fluid Mech., 11*, 317-338, 1979.

Lovelock, J. E., and G. E. Ferber, Exotic tracers for atmospheric studies. *Atmos. Environ., 16*, 1467-1471, 1982.

Maiss, M., and L. Levin, Global increase of SF_6 observed in the atmosphere, *Geophys. Res. Lett., 21*, 569-572, 1994.

McDougall, T. J., Thermobaricity, cabbeling, and water mass conversion, *J. Geophys. Res., 92*, 5448-5464, 1987.

Moyer, K. A., and R. A. Weller, Observations of surface forcing from the subduction experiment: A comparison with global model products and climatological data sets, *J. Clim., 10*, 2725-2742, 1997.

Munk, W. H., Abyssal recipes, *Deep Sea Res., 13*, 707-730, 1966.

Okubo, A., Oceanic diffusion diagrams, *Deep Sea Res., 18*, 789-802, 1971.

Polzin, K. L., J. M. Toole, and R. W. Schmitt, Finescale parameterizations of turbulent dissipation, *J. Phys. Oceanogr., 25*, 306-328, 1995a.

Polzin, K. L., E. Kunze, R. W. Schmitt, and J. M. Toole, Horizontal mixing associated with small-scale vortices, XXI General Assembly, Intl. Assoc. Phys. Sci. Oceans, Abstracts, p. 176, 1995b.

Polzin, K. L., J. M. Toole, J. R. Ledwell, and R. W. Schmitt, Spatial variability of turbulent mixing in the abyssal ocean, *Science, 276*, 93-96, 1997.

Ruddick, B., and D. Hebert, The mixing of Meddy Sharon, in *Small Scale Turbulence and Mixing in the Ocean*, edited by J.C.J. Nihoul and B.M. Jamart, pp. 517-528, Elsevier, New York, 1988.

Ruddick, B., D. Walsh, and N. Oakey, Variations in apparent mixing efficiency in the North Atlantic Central Water, *J. Phys. Oceanogr., 27*, 2589-2605, 1997.

Schmitt, R. W., Double diffusion in oceanography, *Ann. Rev. Fluid Mech., 26*, 255-285, 1994.

Schmitt, R. W., H. Perkins, J. D. Boyd, and M. C. Stalcup, C-SALT: An investigation of the thermohaline staircase in the western tropical North Atlantic, *Deep Sea Res., 34*, 1655-1665, 1987.

Schmitt, R. W., K. L. Polzin, and J. M. Toole, A comparison of direct turbulence measurements with tracer dispersion in the North Atlantic Tracer Release Experiment. *Eos Trans. AGU*, Ocean Sci. Meet., *75*, 130, 1994.

Schuert, E. A., Turbulent diffusion in the intermediate waters of the North Pacific Ocean, *J. Geophys. Res., 75*, 673-682, 1970.

Sherman, J. T., and R. E. Davis, Observations of temperature microstructure in NATRE, *J. Phys. Oceanogr., 25*, 1913-1929, 1995.

St. Laurent, L., and R. W. Schmitt, The contribution of salt fingers to vertical mixing in the North Atlantic Tracer Release Experiment, *J. Phys. Oceanogr.*, in press, 1998.

Sundermeyer, M. A., and J. F. Price, Lateral mixing and the North Atlantic Tracer Release Experiment: Observations and numerical simulations of Lagrangian particles and a passive tracer, *J. Geophys. Res.*, this issue.

Thiele, G., W. Roether, P. Schlosser, R. Kuntz, G. Siedler, and L. Stramma, Baroclinic flow and transient tracer fields in the Canary-Cape Verde Basin, *J. Geophys. Res., 16*, 814-826, 1986.

Toole, J. M., K. L. Polzin, and R. W. Schmitt, Estimates of diapycnal mixing in the abyssal ocean, *Science, 264*, 1120-1123, 1994.

Townsend, A. A., The diffusion of heat spots in isotropic turbulence, *Proc. R. Soc. London, Ser. A, 209*, 418-430, 1951.

Vasholz, D. P., and L. J. Crawford, Dye dispersion in the seasonal thermocline, *J. Phys. Oceanogr., 15*, 695-712, 1985.

Wanninkhof, R., J. R. Ledwell, and A. J. Watson, Analysis of sulfur hexafluoride in seawater, *J. Geophys. Res., 96*, 8733-8740, 1991.

Watson, A. J., and M. I. Liddicoat, Recent history of atmospheric trace gas concentrations deduced from measurements in the deep sea: Application to sulfur hexafluoride and carbon tetrachloride, *Atmos. Environ., 19*, 1447-1484, 1985.

Watson, A. J., M. I. Liddicoat, and J. R. Ledwell, Perfluorodecalin and sulphur hexafluoride as purposeful marine tracers: Some deployment and analysis techniques, *Deep Sea Res., 34*, 19-31, 1987.

Watson, A. J., J. R. Ledwell, and S. C. Sutherland, The Santa Monica Basin tracer experiment: Comparison of release methods and performance of perfluorodecalin and sulfur hexafluoride, *J. Geophys. Res., 96*, 8719-8725, 1991.

Welander, P., An advective model of the ocean thermocline, *Tellus, 11*, 309-318, 1959.

Woods, J. D., Wave-induced shear instability in the summer thermocline, *J. Fluid Mech., 32*, 791-800, 1968.

Young, W. R., P. B. Rhines, and C. J. R. Garrett, Shear flow dispersion, internal waves and horizontal mixing in the ocean, *J. Phys. Oceanogr., 12*, 515-517, 1982.

Clifford S. Law, Plymouth Marine Laboratory, Plymouth, England, United Kingdom. (e-mail: c.law@pml.ac.uk)

James R. Ledwell, Department of Applied Ocean Physics and Engineering, Woods Hole Oceanographic Institution, Woods Hole, MA 02543. (e-mail: jledwell@whoi.edu)

Andrew J. Watson, School of Environmental Sciences, University of East Anglia, Norwich, England, United Kingdom. (e-mail: a.j.watson@uea.ac.uk)

(Received July 16, 1997; revised March 13, 1998; accepted March 31, 1998.)